
When pre-training hurts LoRA fine-tuning: a dynamical analysis via single-index models

Gibbs Nwemadji¹ Bruno Loureiro² Jean Barbier³

Abstract

Pre-training on a source task is usually expected to facilitate fine-tuning on similar downstream problems. In this work, we mathematically show that this naive intuition is not always true: excessive pre-training can computationally *slow down* fine-tuning optimization. We study this phenomenon for low-rank adaptation (LoRA) fine-tuning on single-index models trained under one-pass SGD. Leveraging a summary statistics description of the fine-tuning dynamics, we precisely characterize how the convergence rate depends on the initial fine-tuning alignment and the degree of non-linearity of the target task. The key take away is that even when the pre-training and downstream tasks are well aligned, strong pre-training can induce a prolonged search phase and hinder convergence. Our theory thus provides a unified picture of how pre-training strength and task difficulty jointly shape the dynamics and limitations of LoRA fine-tuning in a nontrivial tractable model.

1. Introduction

Recent advances in machine learning have established pre-trained models as a central paradigm for solving a wide range of tasks (Han et al., 2021). Rather than training models from scratch, modern approaches increasingly rely on adapting a fixed, pre-trained representation using limited task-specific data (Qiu et al., 2020; Han et al., 2021). This trend is particularly pronounced for large language models (LLMs) but extends more broadly. Beyond their empirical performance, pre-trained models offer practical advantages, including reduced computational cost and faster convergence. These benefits have motivated the development of *parameter-efficient fine-tuning* (PEFT) methods (Houlsby et al., 2019; Xu et al., 2023), which aim to adapt large models while updating only a small subset of parameters.

¹International School of Advanced Studies, Trieste, Italy

²Departement d’Informatique, École Normale Supérieure, PSL

& CNRS ³The Abdus Salam International Centre for Theoretical Physics, Trieste, Italy.

Among PEFT methods, *Low-Rank Adaptation* (LoRA) (Hu et al., 2022) has been widely adopted. In this framework, a pre-trained model is adapted to a downstream task by learning a low-rank update of a subset of choice of the weight matrices, while keeping the remaining parameters fixed (Hu et al., 2022; Dettmers et al., 2023). Formally, consider a neural network mapping an input \mathbf{x} to an output via $f(\mathbf{x}; \theta)$, where θ denotes the set of model parameters. Let $\tilde{\omega} \in \mathbb{R}^{K \times d}$ denote a specific pre-trained weight matrix within θ —for instance, an attention or projection layer—to which LoRA is applied (in practice, LoRA can be applied simultaneously to multiple matrices). In this setting, $\tilde{\omega}$ is adapted by learning a low-rank correction of the form $\mathbf{U}\omega$, where $\mathbf{U} \in \mathbb{R}^{K \times R}$ and $\omega \in \mathbb{R}^{R \times d}$ are trainable matrices with $R \ll \min\{K, d\}$. The adapted model can be written as

$$f_{\tilde{\omega}}(\mathbf{x}; \mathbf{U}, \omega) := f(\mathbf{x}; \theta \setminus \{\tilde{\omega}\} \cup \{\tilde{\omega} + \mathbf{U}\omega\}). \quad (1)$$

Compared to full fine-tuning which updates all $k \times d$ entries of $\tilde{\omega}$, LoRA reduces the number of trainable parameters to $(K + d)R$, yielding significant computational savings when R is small. Crucially, the pre-trained matrix $\tilde{\omega}$ is assumed to have been learned from diverse data, and therefore to encode representations that are informative for the downstream task. Understanding the interplay between the pre-trained weights and the low-rank fine-tuning update is critical to the development of a principled understanding of LoRA.

Despite its remarkable success (Yang et al., 2024; Mao et al., 2025), LoRA is only partially understood. While recent studies have begun to characterize its expressive power, convergence properties, and optimization behavior (Zeng & Lee, 2023; Mu & Klabjan, 2025; Kratsios et al., 2025; Liang et al., 2025; Kim et al., 2025; Xu et al., 2025; Zhang et al., 2025), several fundamental questions remain open. In particular, an important one is *how the pre-trained representations impact the LoRA fine-tuning*.

In this work we address this question in the context of single-index models, focusing on the particular role the pre-trained weights play on the fine-tuning learning dynamics. Single-index models define a class of target functions $f_{\star}(\mathbf{x}) = \phi(\omega_{\star} \cdot \mathbf{x})$ in which the relevant information for prediction effectively lies on a one-dimensional subspace of \mathbb{R}^d . It has recently gained in popularity as a non-linear but analytically

tractable model for studying non-convex optimization and feature learning in high-dimensional learning (Gardner & Derrida, 1989; Barbier et al., 2019; Ben Arous et al., 2021; Damian et al., 2022; Ba et al., 2022; Cui et al., 2024; Dandi et al., 2024a). Ben Arous et al. (2021) has shown that the convergence rate of one-pass SGD for single-index models is polynomial in the dimension $n = \Theta(d^{k^*-1})$, with k^* being the *information exponent*, quantifying the degree of non-linearity of activation ϕ . This sample complexity is far from optimal, with $n = \Theta(d)$ typically sufficing for efficiently retrieving ω_* for most well-behaved ϕ (Kalai & Sastry, 2009; Barbier et al., 2019; Damian et al., 2024).

In this manuscript, we build on this literature to investigate the question of how the initial alignment of the pre-trained weights impact the LoRA fine-tuning under one-pass SGD. We analyze the optimization process, with particular emphasis on the early-stage *search phase*, during which the model must identify the relevant direction in the data. This provides an algorithmic perspective on LoRA that complements existing statistical guarantees. More precisely, our **main contributions** are three-fold:

- First, we quantify how the degree of alignment between the pre-trained representation and the downstream task governs the time required to escape the search phase. Surprisingly, we show that for commonly used activation functions—such as linear, erf, ReLU, and sigmoid—a *trade-off* exists between the improved initial performance due to pre-training and the algorithmic tractability of further finite-tuning with LoRA: strongly aligned pre-training can slow down the learning dynamics rather than accelerate it as intuition may suggest (see Figure 1). This effect mirrors recent empirical observations in LLMs by Springer et al. (2025) and Isik et al. (2025) known as *catastrophic overtraining*.
- Second, we identify settings—determined jointly by the level of pre-training alignment and the activation function—in which escape from the search phase is provably impossible.
- Third, we study whether label transformations can accelerate escape, and clarify the role of such pre-processing in our transfer-learning setting.

Additional related work. A growing literature has recently begun to establish rigorous theoretical foundations for LoRA (Hu et al., 2022). Early work by Zeng & Lee (2023) characterized rank conditions under which LoRA can accurately approximate a target function. In the neural tangent kernel (NTK) regime, Jang et al. (2024) showed that for ranks $R \geq \sqrt{n}$ —where R denotes the LoRA rank and n the sample size—the loss landscape contains no spurious local minima. Beyond asymptotic analyses, Mu & Klabjan

(2025) proved that, for a finite number of gradient steps, the convergence rate of LoRA is independent of the rank, although the limit point may differ substantially from that of full-rank gradient descent. Related studies (Hayou et al., 2024; Kim et al., 2025; Xu et al., 2025) highlighted the role of zero initialization in biasing the dynamics toward regions containing global minima, while Zhang et al. (2025) demonstrated that, under carefully chosen initializations, a single gradient step may suffice for recovery. In an asymmetric setting where only one LoRA factor is trained, Kratsios et al. (2025) showed that the generalization error scales as $O(\sqrt{R/n})$ with high probability (up to polylog factors). A common limitation across these works is that pre-trained weights are typically modeled as random or unstructured, and therefore not explicitly aligned with the downstream task, leaving the role of task-relevant pre-training largely unexplored. Our work participates to fill this gap in the context of single-index models.

2. Setting

We study a tractable yet non-trivial teacher–student model that captures the essential structure of LoRA-based transfer learning on a non-linear, non-convex task. More precisely, we assume the target function is a single-index model of the form $f_*(\mathbf{x}) = \phi(\omega_* \cdot \mathbf{x})$, where $\omega_* \in \mathbb{S}^{d-1}$ is an unknown unit vector and $\mathbf{x} \in \mathbb{R}^d$ is the input data. We observe a dataset $\mathcal{D} = \{(\mathbf{x}_i, y_i)\}_{i=1}^n$ consisting of conditionally (on ω_*) i.i.d. samples, with inputs $\mathbf{x}_i \sim \mathcal{N}(0, I_d)$ and labels

$$y_i = \phi(\omega_* \cdot \mathbf{x}_i). \quad (2)$$

In analogy with LoRA, we consider a student model obtained by updating a pre-trained direction with limited signal strength, i.e., we study predictors of the form:

$$f_{\tilde{\omega}}(\mathbf{x}_i; u, \omega) = \sigma((\tilde{\omega} + u\omega) \cdot \mathbf{x}_i), \quad (3)$$

where the learnable parameters consist of a scalar $u \in \mathbb{R}$ and a direction $\omega \in \mathbb{S}^{d-1}$. The vector $\tilde{\omega} \in \mathbb{R}^d$ represents a feature direction inherited from pre-training and is assumed to be aligned with the target direction ω_* . A natural choice is therefore $\tilde{\omega} := \mu\omega_*$, where the parameter $\mu \in (0, 1)$ quantifies the amount of prior information carried by the pre-trained model. In App. A.1, we show that this encompasses also misaligned pre-trained weights such $\tilde{\omega} = \mu\omega_* + (1 - \mu)\xi$ without loss of generality.

This formulation corresponds to a transfer-learning scenario in which pre-training yields an informative but imperfect representation for the downstream task, here given by (2). Fine-tuning on the dataset \mathcal{D} then improves performance beyond what is achievable with the pre-trained weights alone, via the rank-one correction $u\omega$. Throughout this work, we assume that both the target $\phi(\cdot)$ and are square-integrable with respect to the standard Gaussian measure.

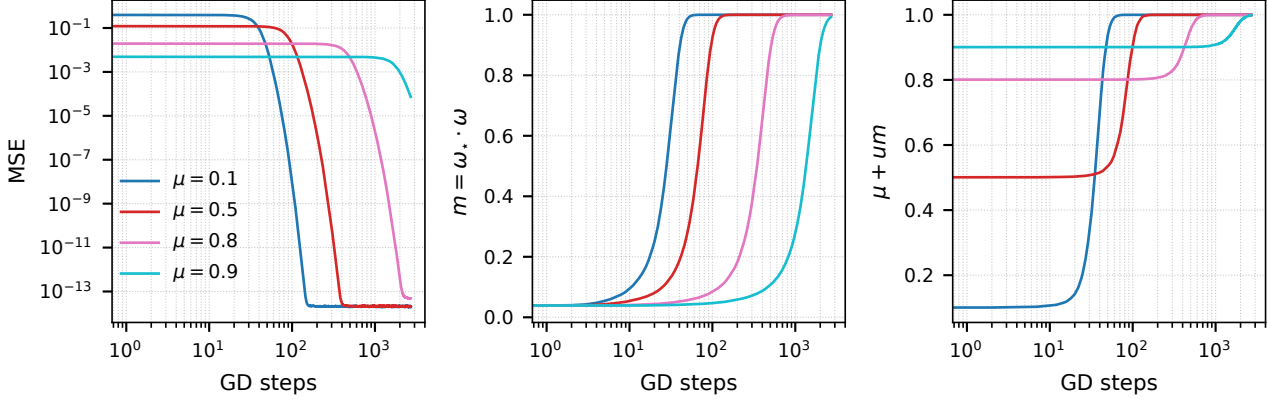


Figure 1. Learning dynamics of the student model (3) for different levels of pre-training alignment $\mu \in \{0.1, 0.5, 0.8, 0.9\}$, trained on data generated by the teacher model (2). We consider the matched teacher–student linear activation setting and train the student using one-pass SGD with batch size $B = 500$ and input dimension $d = 1000$. The panels report the test mean squared error (MSE) (left), the alignment between the student and teacher directions $m = \omega_* \cdot \omega$ (middle), and the effective teacher–student overlap $m_{\text{eff}} = \mu + um$ (right). Shaded regions indicate one standard deviation over three independent runs. The spherical constraint is enforced by normalizing ω after each gradient step. Additional results for Erf, ReLU, and Sigmoid activations are reported in Appendix E.3.

It is worth noting that (Springer et al., 2025) provides theoretical grounds to quantify *catastrophic overtraining*, but their analysis is limited to linear models and relies on an explicit alignment penalty to model weight transfer. As a result, it abstracts away from unconstrained fine-tuning as commonly used in practice and does not incorporate PEFT methods. In parallel, (Isik et al., 2025) show that downstream performance may fail to scale monotonically with pre-training when source and target tasks are poorly aligned. In contrast, even when pre-training and downstream tasks are explicitly aligned, our framework exhibits a significant delay in learning induced by stronger pre-training.

2.1. One-pass stochastic gradient descent

Given a dataset $\mathcal{D} = \{(\mathbf{x}_i, y_i)\}_{i=1}^n$ of n samples drawn from model Equation (2), we are interested in the fine-tuning training dynamics of (u, ω) with *spherical one-pass SGD*:

$$\omega^{i+1} = \frac{\omega^i - \gamma \nabla_{\omega} (y_i - f_{\bar{\omega}}(\mathbf{x}_i; u^i, \omega^i))^2}{\|\omega^i - \gamma \nabla_{\omega} (y_i - f_{\bar{\omega}}(\mathbf{x}_i; u^i, \omega^i))^2\|}, \quad (4)$$

$$u^{i+1} = u^i - \gamma \nabla_u (y_i - f_{\bar{\omega}}(\mathbf{x}_i; u^i, \omega^i))^2 \quad (5)$$

where $\gamma > 0$ is the learning rate and $i \in [n]$. Note that, in line with other works on one-pass SGD for single-index models, the choice of constraining $\omega \in \mathbb{S}^{d-1}$ is mostly for analytical simplicity, and it can be shown it does not impact the dynamics considerably (Ben Arous et al., 2021). Note that one-pass SGD (also known as *streaming* or *online* SGD), sees one sample at a time with no repetition, implying that the convergence rate is equal to the sample complexity of the algorithm.

Since the gradients in Equation (4) are unbiased estimators

of the population gradient, the one-pass dynamics can be seen as a random discretization of gradient flow on the population risk (Robbins & Monro, 1951):

$$\mathcal{L}(u, \omega) = \mathbb{E}[(y - f_{\bar{\omega}}(x; u, \omega))^2] \quad (6)$$

where the expectation is over the pair (x, y) . The key observation for the analysis that will follow is that the population loss in Equation (6) only sees the data through the pre-activations of the target $\lambda_* := \omega_* \cdot x$ and model $\lambda := (\mu \omega_* + u \omega) \cdot x$. Since $x \sim \mathcal{N}(0, I_d)$, the pair (λ_*, λ) is jointly Gaussian with law

$$(\lambda_*, \lambda) \sim \mathcal{N}(0, \Sigma), \quad \Sigma = \begin{pmatrix} 1 & \mu + um \\ \mu + um & r \end{pmatrix},$$

where we have introduced the “overlap” $m := \omega \cdot \omega_*$ and the student pre-activation variance $r := \mu^2 + u^2 + 2\mu um$. An important related quantity is the effective alignment $m_{\text{eff}} := \mu + um$, which measures the total alignment of the model predictor with the target direction and serves as an indicator of recovery.

Order parameters and their dynamics. An important consequence of the discussion above is that the population loss $\mathcal{L}(u, \omega)$ depends on the parameters (u, ω) only through two scalar quantities: the coefficient u and the overlap $m = \omega \cdot \omega_*$. This suggests a reduced description of the high-dimensional learning dynamics in Equation (4) in terms of the evolution of these two summary statistics. Indeed, this reduction will be the key technical tool in the analysis of the convergence rate for the LoRA fine-tuning that will follow.

The evolution of m can be obtained from Equation (4) by projecting the update ω^{i+1} onto the target direction ω_* .

This defines a system of coupled stochastic processes for (m^i, u^i) , which are not autonomous. However, defining $t = \gamma i$ it can be shown that for small enough learning rate γ , this process concentrate on a deterministic limit given by gradient descent on the population loss

$$(m^{t+1}, u^{t+1}) = (m^t, u^t) - \gamma \nabla \tilde{\mathcal{L}}(u^t, m^t) + O(\gamma^2),$$

where $\tilde{\mathcal{L}}(u, m)$ denotes the population loss expressed solely in terms of (u, m) . We refer the reader to Appendix C for details. For simplicity, we will henceforth use $\mathcal{L}(u, m)$ to denote this reduced loss.

We note that similar ideas, rooted in the statistical physics of learning literature have been employed in wide range of contexts in the study the one-pass SGD dynamics in machine learning (Saad & Solla, 1996; Goldt et al., 2019; 2020; Veiga et al., 2022; Arnaboldi et al., 2023b;a; Saglietti et al., 2022; Mori et al., 2025; Soletskyi et al., 2025).

We consider initial conditions consistent with standard LoRA practice. In applications, the scalar parameter u is typically initialized at zero (Hu et al., 2022; Dettmers et al., 2023; Yang et al., 2024), while the student direction ω is chosen at random. In the high-dimensional limit $d \rightarrow \infty$, such a random initialization yields an initial overlap $m = \omega \cdot \omega_* = O(d^{-1/2})$ with high probability. For analytical convenience, and in order to obtain a nontrivial joint evolution of the order parameters, we therefore assume that both u and m are initialized at scale $d^{-1/2}$. This scaling remains asymptotically close to the standard initialization used in practice. Consistently, recent works (Hayou et al., 2024; Kim et al., 2025; Xu et al., 2025) show that small initialization of the LoRA block leads to improved generalization error.

2.2. Hermite expansion and learning phases

In the standard well-specified $\sigma(\cdot) = \phi(\cdot)$ single-index model, Ben Arous et al. (2021) has shown that the convergence rate of one-pass SGD in the high-dimensional and small learning rate regime is given by $n = \Theta(d^{k^*-1})$, where k^* is the *information exponent* (IE) associated to the activation function, defined as the smallest non-zero term $k^* \geq 1$ in the Hermite expansion of the activation function ϕ . Indeed, this is intuitive, as k^* quantifies the strength of the leading gradient signal available at the early phases of SGD.

In our fine-tuning setting, model and target may have different pre-activation variances, which requires a generalized Hermite expansion. Let $a > 0$ denote the variance of a Gaussian pre-activation, and assume that $\mathbb{E}[\sigma(z)^2] < \infty$ for $z \sim \mathcal{N}(0, a)$. Then σ admits the expansion

$$\sigma(z) = \sum_{k \geq 0} \frac{\sigma_k^{[a]}}{k! a^k} \text{He}_k^{[a]}(z), \quad (7)$$

with details on $\sigma_k^{[a]}$ and $\text{He}_k^{[a]}$ —that denotes the k -th Hermite polynomial—available in App. B.1. The teacher activation operates at unit variance, and thus admits a standard Hermite expansion $\phi(z) = \sum_{k \geq 0} \frac{\phi_k}{k!} \text{He}_k(z)$. The mismatch between the pre-activation variances of the target and model plays a nontrivial role in shaping the IE of the model. To illustrate this effect, we consider the well-specified setting $\sigma(\cdot) = \phi(\cdot)$ and assume, for simplicity, that the activation function is a pure Hermite polynomial of degree $k^* \geq 2$ corresponding to having a target with IE $= k^*$. In our student model, the pre-activation variance is $r = r(u, m, \mu) := \mu^2 + u^2 + 2\mu um$, which is generically different from 1. As a consequence, the Hermite expansion of the student possesses nonzero coefficients only for Hermite polynomials whose degrees match the parity of k^* , thereby inducing an effective reduction of the student's IE to at most 2, independently of that of the teacher. In particular, this analysis suggests that a byproduct of learning within the LoRA framework is an implicit regularization of the IE to at most 2. A detailed derivation of this variance-induced IE reduction is provided in App. B.3.

Using the generalized Hermite expansion (7), together with the detailed computations presented in App. B.2, the population loss can be written explicitly as

$$\mathcal{L}(u, m) = \sum_{k=0}^{\infty} \frac{1}{k!} \left(\frac{\phi_k^2}{2} + \frac{(\sigma_k^{[r]})^2}{2r^k} - \frac{\sigma_k^{[r]}\phi_k}{r^k} (\mu + um)^k \right).$$

Although the second term depends on (u, m) via $r(u, m, \mu)$, it simply acts as an effective regularization (it corresponds to the term in the loss depending on the student only). Hence, learning of task-relevant structure is driven by the third term, which governs the sample complexity. When the teacher has IE $= k^*$, the leading nonzero contribution of this term scales as $m_{\text{eff}}^{k^*} = (\mu + um)^{k^*}$, while higher-order terms scale as $m_{\text{eff}}^{k^*+p}$ for $p \in \mathbb{N}_+$. In the setting of Ben Arous et al. (2021) ($\mu = 0, u = 1$), one has $m_{\text{eff}} = m \ll 1$ at early times, so higher-order terms are suppressed and the loss is well approximated by its leading Hermite component. In contrast, when $\mu \neq 0$, although um remains infinitesimal initially, $m_{\text{eff}} = O(1)$ due to μ , making higher-order contributions non-negligible. As a result, the population loss cannot be truncated to its leading Hermite term, showing that *the IE alone is insufficient* to characterize the loss near initialization in the presence of pre-training.

Learning phases. Our analysis reveals the existence of two distinct phases in the evolution of the order parameters, which are clearly illustrated by simulations (see Figure 1):

- *Correlated search phase:* the dynamics starts from a weakly correlated regime in which the order parameters satisfy $\max(|u|, |m|) \ll \mu$, though the effective teacher-student overlap satisfies $m_{\text{eff}} \simeq \mu$.

- *Descent phase*: once the process enters this regime, at least one of the order parameters becomes comparable to the signal strength, i.e. $|m| \geq \mu$ and/or $|u| \geq \mu$.

In Ben Arous et al. (2021), Thm. 1.5 shows that the majority of samples/updates are used during the search phase, while, once this phase is exited, the model recovers the target direction at an exponential rate in time, making the search phase the most algorithmically relevant regime. This is in sharp contrast to our setting, where the model has finite correlation $\mu > 0$ with the target vector ω_* at initialization and hence throughout the full trajectory, so that the search dynamics remain correlated. Our main results (see Section 3) provide a fine-grained analysis of how the signal strength μ and the choice of the activation function affect the phenomenology of this correlated search phase. Moreover, we establish in App. G that, upon entering the descent phase, the dynamics still lead to exponential recovery of the teacher direction for matching teacher-student activation function.

3. Main results

In the correlated search phase, both u and m remain small compared to μ , which implies that the drift of the dynamics is governed by the leading-order dependence of the population-loss gradients on (u, m) . We therefore linearize the gradient of its full Hermite expansion, keeping only terms proportional to u and m . In the infinitesimal learning-rate limit, this leads to the following linearized dynamics for the order parameters:

$$\dot{u} = uB + mA, \quad \dot{m} = uA, \quad (8)$$

with

$$A = - \sum_{k=0}^{\infty} \frac{\bar{\sigma}_k^{[r]}}{k! \mu^{k+1}} \left(-\phi_k + \frac{\sigma_k^{[r]}}{\mu^k} \right), \quad (9)$$

$$B = - \left[\sum_{k=0}^{\infty} \frac{\bar{\sigma}_k^{[r]} \sigma_k^{[r]}}{k! \mu^{2k+2}} + \sum_{k=1}^{\infty} \frac{\phi_k}{(k-1)! \mu^{k+2}} \left(\sigma_k^{[r]} - \frac{\bar{\sigma}_k^{[r]}}{k} \right) \right]$$

with $\bar{\sigma}_k^{[r]}$ defined in App. D.1 and derivations details are provided in the App. D.2 and E.1. Note that for $A \neq 0$ there is no solution in which u or m evolves independently: any infinitesimal deviation from the origin immediately induces coupled dynamics in both variables.

3.1. Escaping time

Using the linearized gradient dynamics in (u, m) , one would expect the exit time t_{exit} —defined as the time at which at least one of the order parameters becomes comparable to the signal strength, i.e. $|u| = \Theta(\mu)$ and/or $|m| = \Theta(\mu)$ —to scale at most as $O(\log d)$, in line with the analysis of Ben Arous et al. (2021) for $\text{IE} = 2$. However this intuition is not always correct: depending on the choice of the

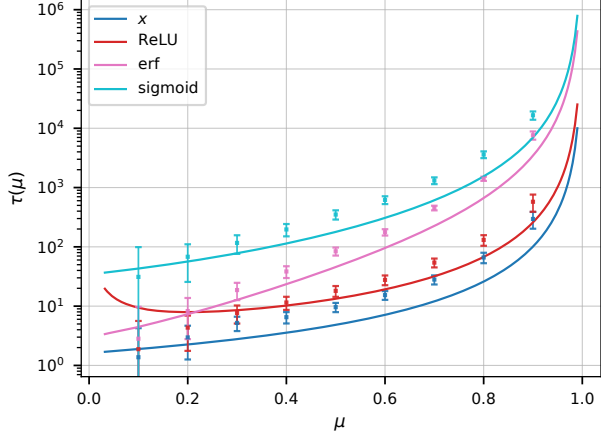


Figure 2. Theoretical predictions of the characteristic escape time $\tau(\mu)$ (solid lines) and corresponding numerical estimates (markers) for the time required to exit the correlated search phase of the student model (3) trained on data generated by the teacher model (2). Results are shown for matched teacher-student activation functions that have $\text{IE} = 1$. Numerical results have been obtained by running one-pass SGD with batch-size $B = 500$, input dimension $d = 1000$, learning rate = 0.2 and we average over three instances of the experiment. We record the numerical escape time τ_{exp} at the point where the overlap reaches $m \simeq 0.98$ for all functions, since the descent phase proceeds exponentially fast (cf. Fig. 7).

activation function, the learning dynamics may fail to escape the correlated search phase because of the pre-training. We capture this phenomenon by providing a sharper characterization of t_{exit} that makes its dependence on the drift coefficients A, B explicit. From now on, for sequences $a = a_d$ and $b = b_d$ we write $a \sim_d b$ if $\lim_{d \rightarrow \infty} a/b = 1$.

Proposition 1 (Exit time from the correlated search phase). *Assume that $A \neq 0$. Then the time at which the dynamics escapes the correlated search phase satisfies*

$$t_{\text{exit}} \sim_d \frac{\tau(\mu)}{2} \log d, \quad \tau(\mu) = \frac{-B + \sqrt{B^2 + 4A^2}}{2A^2}, \quad (10)$$

with A, B given in (9) depend on the teacher and student activation functions $\sigma(\cdot), \phi(\cdot)$ and on the signal strength μ .

Remark 1. Prop. 1 shows that the exit time scales as $A^{-2} \log d$. Consequently, small values of A and $B < 0$ substantially slow down the transition out of the correlated search phase. In particular, if for some choice of teacher-student activation functions and μ one has $A = 0$, then the ratio $t_{\text{exit}} / \log d$ diverges. This corresponds to a regime in which the dynamics fails to escape the correlated search phase despite the presence of non-zero initial correlation. The proof is provided in App. E.1.

3.2. Well-specified activation function

Although we argued that the IE is not enough to characterize the population loss, we nevertheless use it here as a guiding descriptor of the chosen activation function. Our conclusions should therefore be understood as statements about the specific activation considered, rather than about the entire class of functions sharing the same IE.

(a) Linear activation function. We first consider the linear case $\sigma(x) = \phi(x) = x$. As expected, larger values of μ yield smaller initial test mean squared error, reflecting stronger initial alignment with the teacher (left panel of Fig. 1). However, a striking phenomenon emerges during training: despite their worse initial performance, models initialized with smaller signal strength μ converge to the global optimum significantly faster: highly pre-trained models (e.g. $\mu = 0.9$) exhibit a pronounced delay before convergence. This behavior is clearly visible in the evolution of the overlap m (middle panel of Fig. 1), where models with larger μ remain trapped in the correlated search phase for substantially longer times. The same effect is reflected in the effective alignment m_{eff} (right panel of Fig. 1). Our theory accounts for this trade-off between initial, pre-trained performance and algorithmic tractability of the downstream LoRA fine-tuning. Since the characteristic time $\tau(\mu)$ determines the exit time t_{exit} (Prop. 1), Fig. 2 shows that $\tau(\mu)$ indeed increases monotonically with μ . This slowdown is driven by the drift coefficient A controlling the evolution of m , which for linear activation scales as $A \propto 1 - \mu$ (App. E.2). Consequently, stronger pre-trained alignment weakens the effective gradient signal along the teacher direction, delaying escape from the correlated search phase. We provide in App. F a physics-inspired explanation of this phenomenon. A related phenomenon has been observed in the context of LLMs (Springer et al., 2025), where excessive pre-training, corresponding to increasing the amount of pre-training data, is shown to impair downstream performance.

(b) Activation functions with IE = 1. We next consider commonly used activations with IE = 1, including erf, sigmoid, and ReLU. Overall, the qualitative behavior observed for the linear activation function largely persists: increasing the signal strength μ typically leads to longer residence times in the correlated search phase. For erf and sigmoid, Fig. 2 shows that $\tau(\mu)$ governing escape grows monotonically with μ . ReLU exhibits a mild deviation from this monotone trend at relatively small signal strengths: as μ increases from 0 to 0.2, $\tau(\mu)$ decreases slightly, suggesting that a weakly more informative pre-trained weight can initially accelerate escape. However, once μ exceeds 0.2, the behavior aligns with the other activations. A common feature across all these activation functions is the divergence of the $\tau(\mu)$ as $\mu \rightarrow 1^-$, implying that highly corre-

lated pre-trained weights require substantially more gradient steps—and, in the online regime, substantially more fresh data—before the dynamics can leave the correlated search phase. Finally, for all $\text{IE} = 1$ activations considered here, the escape-time curves appear continuous over $\mu \in (0, 1)$: escape occurs for any fixed $\mu \in (0, 1)$, but the associated time scale depends sensitively on both μ and the choice of activation function.

(c) Beyond IE = 1. We now consider activation functions with $\text{IE} \geq 2$, which in the standard, non-fine tuning case, are known to be harder to learn. As shown in Ben Arous et al. (2021); Damian et al. (2023), the duration of the search phase for such activations grows as a power of the IE. Our objective here is to assess how increasing the activation function complexity qualitatively alters the correlated search dynamics relative to the setting studied in Ben Arous et al. (2021). To this end, we focus on pure Hermite activation functions—whose Hermite degree coincides with their IE—and distinguish between odd and even degrees, which exhibit qualitatively different behaviors.

– **Odd Hermite activation functions.** For pure Hermite activations of odd degree, the following proposition holds.

Proposition 2. *Consider the well-specified setting $\sigma = \phi$ with pure Hermite activation function $\sigma(z) = \text{He}_k(z)$ of odd degree $k \geq 3$. Let $A(\mu)$ be as in (9). There exists at least one $\tilde{\mu} \in (0, 1)$ such that $A(\tilde{\mu}) = 0$. Thus at $\mu = \tilde{\mu}$ the exit time $t_{\text{exit}} \sim_d (\tau(\tilde{\mu}) \log d)/2$ diverges.*

Prop. 2 shows that, in contrast to all activation functions considered so far, for pure odd Hermite activations there exist at least one nonzero value of the pre-training alignment $\tilde{\mu}$ for which the learner cannot escape the correlated search phase despite the initial correlation. The proof is in App. E.4 Using Prop. 1, we can further refine the location of the singularity guaranteed by Prop. 2. Indeed, in the bottom panel of Figure 3, we observe the divergence of t_{exit} for pure odd Hermite activation functions. This critical value shifts to the right as the degree of the Hermite polynomial increases. On both sides of this singularity, t_{exit} exhibits a parabola-like behavior, with again divergences as $\mu \rightarrow 0^+$ and $\mu \rightarrow 1^-$. Interestingly, as $\mu \rightarrow 1^-$, higher Hermite degrees yield a faster escape than lower ones, a counterintuitive behavior given the findings of Ben Arous et al. (2021). This qualitative behavior is reversed in the regime $\mu \rightarrow 0^+$, which agrees with Ben Arous et al. (2021). Prop. 3 provides quantitative results for these extremes. In the inset of Fig. 3, we provide numerical results for Hermite He_3 showing the dynamic of m across epoch for $\mu \in \{0.2, 0.325\}$. This confirms that the dynamics indeed take a significantly longer time for $\mu = 0.325$, which is close to the singularity, compared to $\mu = 0.2$. Further details on other observables can be found in App. J.

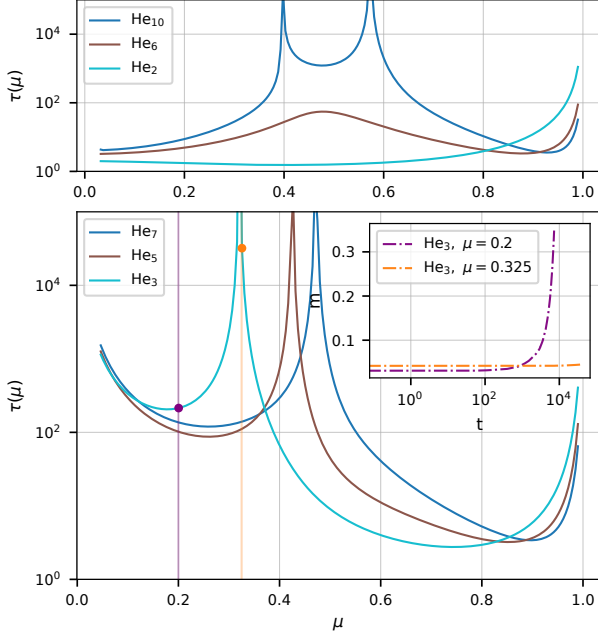


Figure 3. Theoretical predictions of the characteristic escape time $\tau(\mu)$ (solid lines) for exiting the correlated search phase of the student model (3) trained on data generated by the teacher model (2). Results correspond to matched teacher–student Hermite activations He_k (see legend). In the bottom panel, the vertical lines and corresponding dots indicate the specific values of μ at which numerical simulations are performed and reported in the inset. The inset shows the numerical evolution of the overlap m for He_3 , obtained using one-pass SGD with batch size $B = 500$, input dimension $d = 1000$, and learning rate 5.5×10^{-5} , at $\mu \in \{0.2, 0.325\}$ and averaged over three independent runs. These results confirm that, near the singular region $\mu = 0.325$ (highlighted by the orange dot), the dynamics require substantially longer times to escape.

– Even Hermite activation functions. Using Prop. 1, we observe that for even Hermite degrees that are sufficiently large, two singularities appear. Indeed, as shown in the top panel of Fig. 3, where $\tau(\mu)$ is reported for pure even Hermite activation functions, no singularity is observed for He_2 and He_6 , whereas clear singularities emerge for He_{10} . The behavior as $\mu \rightarrow 1^-$ is qualitatively similar to that observed in the odd Hermite case. A distinct regime emerges, however, as $\mu \rightarrow 0^+$: $\tau(\mu)$ remains finite across all degrees, a fact for which Prop. 3 provides a mathematical guarantee. This behavior is the result of the presence of a nonzero mean on the model—suggesting that the mean is easy to learn even for vanishing μ —induced by such activations, whose magnitude increases with the Hermite degree but vanishes in the limit $\mu \rightarrow 1$; see App. E.5 for a formal analysis. Numerically (cf. Appendix E.5), we further observe that for moderate signal strengths $\mu \leq 0.2$, the dynamics exit the correlated search phase rapidly, in agreement with theoretical predictions, but subsequently enter an extended

plateau in the evolution of u , while the overlap m continues to grow. Once u leaves this plateau, convergence toward the global minimizer becomes rapid. This intermediate stagnation regime is specific to even Hermite activations and suggests that the mean component is learned quickly, whereas higher-order features are learned much later. Since the model has zero mean when using odd Hermite activations, this behavior is not observed in that case; supporting numerical evidence is reported in App. E.5.

– Pure Hermite activations in extreme pre-training regimes. We now consider the extreme cases in which the pre-trained weights are either highly aligned or extremely weakly aligned with the target direction. For functions $a = a(\mu)$ and $b = b(\mu)$, $a \sim_\mu b$ means $\lim_{\mu \rightarrow \mu_0} a/b = 1$.

Proposition 3. Consider the matching teacher–student setting $\sigma = \phi$ with a pure Hermite activation function of degree $k \geq 1$, $\sigma(z) = \text{He}_k(z)$ with $k \geq 3$. Let $\tau(\mu)$ be the characteristic prefactor of t_{exit} appearing in the scaling (10) of Prop. 1. Then the following asymptotics hold:

- With strong alignment $\mu \rightarrow 1^-$,

$$\tau(\mu) \sim_\mu \frac{4}{(2k-1)^2} \frac{1}{(\mu^2 - 1)^2}.$$

- With weak alignment $\mu \rightarrow 0^+$,

$$\tau(\mu) \sim_\mu \begin{cases} B_0^{-1}, & \text{if } k = 2p \text{ with } p \in \mathbb{N}, p \geq 1, \\ -\frac{B_0}{c_p \mu^2}, & \text{if } k = 2p + 1 \text{ with } p \in \mathbb{N}, p \geq 1, \end{cases}$$

where $B_0 = \lim_{\mu \rightarrow 0^+} B(\mu)$ is finite (recall (9)) and $c_p^{-1} = p!(p-1)!2^{2p-1}/(2p-1)!$.

This result provides fine-grained analysis of observation made in Fig. 3. For μ near one, higher-degree Hermite activation functions can escape the correlated search phase faster than lower one despite having a larger IE (and thus being harder to learn in the standard setting). In contrast, near zero, odd and even degrees behave differently, with odd degrees exhibiting a pronounced slowdown (see numerics in Fig. 3 of App. E.5). Taken together, these scalings clarify how the interplay between pre-training strength and activation function complexity reshapes the search dynamics. The proof of Prop. 3 is done in App. E.4.

3.3. Misspecified activation functions

As discussed in the introduction, when $\text{IE} > 2$, there exists a fundamental gap between the sample complexity of one-pass SGD and that of optimal algorithms for weakly learning single-index models. This gap stems from the fact that, at initialization, SGD gradients are both independent and weak. In particular, one-pass SGD updates can be viewed as CSQ

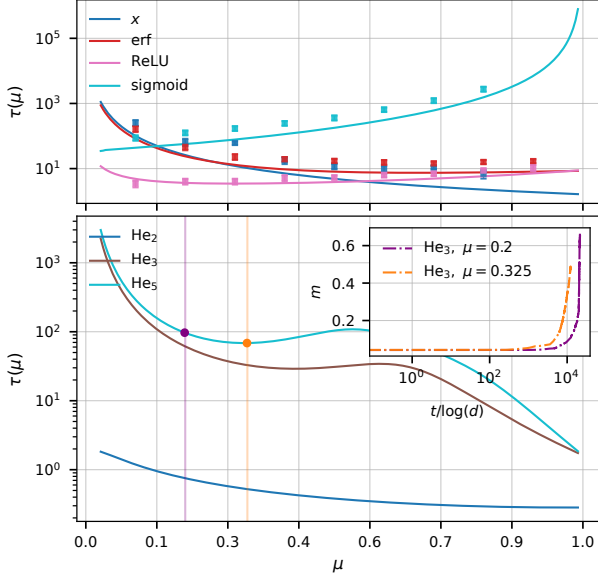


Figure 4. Theoretical predictions (solid lines) of the characteristic escape time $\tau(\mu)$ in a setting where labels generated by the teacher model (2) are squared before training the student model (3), thereby modifying the information exponent (IE) of the loss. **Top:** for standard activations, this transformation reverses the dependence of $\tau(\mu)$ on the signal strength μ in some cases, while leaving others unchanged. These numerical results are obtained using one-pass SGD with batch size $B = 500$, input dimension $d = 1000$, and learning rate $lr = 0.2$, and are averaged over three independent runs. **Bottom:** for Hermite activations, squaring enforces $IE \leq 2$, removes the singular behavior of $\tau(\mu)$, and induces an approximately monotonic decrease of $\tau(\mu)$ with increasing μ ; vertical lines and corresponding markers indicate the specific values of μ at which numerical simulations are performed. Consistently, the inset shows the numerical evolution of the overlap m at the values of μ highlighted in the main panel, illustrating substantially earlier compare to the unsquared case (cf. Fig. 3), despite identical numerical settings.

queries of the form $\mathbb{E}[y, \varphi(x)]$, for which a general lower bound of $n \gtrsim O(d^{-IE/2})$ holds (Damian et al., 2023). By contrast, iterative algorithms such as AMP (Barbier et al., 2019) or full-batch gradient descent (Dandi et al., 2024b), which typically achieve weak recovery with $n = \tilde{O}(d)$ samples, effectively implement more expressive queries of the form $\mathbb{E}[\psi(y)\varphi(x)]$. These are known as SQ queries and allow for arbitrary transformations of the labels.¹

Therefore, it is natural to ask whether label transformations can speed up the convergence of fine-tuning. Note that transformations of the labels effectively correspond to introducing a mismatch between the target and model ac-

¹The sample complexity lower bound for SQ algorithms $n \gtrsim \tilde{O}(d^{GE/2})$ is instead governed by the so-called *generative exponent*. For most common activation functions ϕ , one has $GE = 2$ (Damian et al., 2024).

tivation functions. A simple transformation that achieves this goal is label squaring. As shown in App. B.4, squaring a pure Hermite polynomial yields a function whose lowest nonzero Hermite component is He_2 , thereby reducing the effective IE to be at most 2. We emphasize that such transformations are not intended to improve the final test mean squared error, but rather to reshape the optimization landscape during the early stage of learning; similar strategies have been employed in related contexts (Damian et al., 2024). Accordingly, once the search phase is exited, we revert to the original labels in order to fully recover the target direction. This resulting two-stage learning strategy—using transformed, or “softened”, labels early and switching back to hard labels thereafter—is widely used in practice, notably in semi-supervised and self-training methods such as FixMatch (Sohn et al., 2020), as well as in curriculum learning approaches (Bengio et al., 2009).

Beyond pure Hermite activations, we also investigate how this transformation affects the phenomenology observed so far for activation functions with $IE = 1$. In the upper panel of Fig. 4, we observe that after applying this transformation to the labels generated by activation functions such as the linear x , ReLU, and erf, the behavior in the correlated search phase is qualitatively *reversed* compared to the matching-activation setting of Fig. 2. In particular, for x and erf, stronger alignment of the pre-trained weight with the target direction (larger μ) now leads to *faster* escape from the correlated search phase, in sharp contrast with the matching-activation case. Moreover, for x , ReLU, and erf, the exit time no longer diverges as $\mu \rightarrow 1^-$, unlike what was observed previously. For the sigmoid activation, squaring the labels has little effect on $\tau(\mu)$, which is expected given that this transformation induces only a mild change in the effective shape of the activation function. The bottom panel of Fig. 4 shows that the general trend observed for $IE \geq 2$ activation functions under this transformation is an *overall decreasing* behavior of $\tau(\mu)$ as μ increases. Most notably, for odd Hermite activation functions, the singularities previously observed in the matching case disappear after squaring the labels, indicating that this transformation smooths the optimization landscape and restores efficient escape from the correlated search phase. Additional numerical evidence demonstrating how these observations can be leveraged to accelerate learning—and, in particular, to bypass singular values of μ —is provided in the App. B.4.

4. Discussion

Our results reveal a non-trivial role of the pre-trained signal: stronger alignment does not necessarily accelerate learning and can, in certain regimes, significantly slow down the dynamics. While our main analysis focuses on single-index models, Appendix I extends these findings to two-layer neu-

ral networks and shows that, during the correlated search phase, escape dynamics are primarily controlled by alignment strength rather than by the LoRA rank, consistent with Mu & Klabjan (2025). Appendix F further provides a physics interpretation that clarifies why stronger alignment can hinder fine-tuning and elucidates the distinct roles of the LoRA components. How rank and pre-training jointly determine final performance remains an open question.

Acknowledgements

We thank Kimia Nadjahi for insightful discussions. G.N. thanks Mauro Pastore for extensive discussions and insightful feedback throughout the development of this work. B.L. was supported by the French government, managed by the National Research Agency (ANR), under the France 2030 program with the reference “ANR-23-IACL-0008” and the Choose France - CNRS AI Rising Talents program. J.B. was funded by the European Union (ERC, CHORAL, project number 101039794). Views and opinions expressed are however those of the authors only and do not necessarily reflect those of the European Union or the European Research Council. Neither the European Union nor the granting authority can be held responsible for them.

Software and Data

The code used for the numerical experiments is publicly available at <https://github.com/GibbsNwemadji/When-pre-training-hurts-LoRA>.

References

Arnaboldi, L., Krzakala, F., Loureiro, B., and Stephan, L. Escaping mediocrity: how two-layer networks learn hard single-index models with sgd. *CoRR*, 2023a.

Arnaboldi, L., Stephan, L., Krzakala, F., and Loureiro, B. From high-dimensional & mean-field dynamics to dimensionless odes: A unifying approach to sgd in two-layers networks. In *The Thirty Sixth Annual Conference on Learning Theory*, pp. 1199–1227. PMLR, 2023b.

Arnaboldi, L., Dandi, Y., Krzakala, F., Pesce, L., and Stephan, L. Repetita iuvant: Data repetition allows sgd to learn high-dimensional multi-index functions. *arXiv preprint arXiv:2405.15459*, 2024.

Ba, J., Erdogdu, M. A., Suzuki, T., Wang, Z., Wu, D., and Yang, G. High-dimensional asymptotics of feature learning: How one gradient step improves the representation. *Advances in Neural Information Processing Systems*, 35: 37932–37946, 2022.

Barbier, J., Krzakala, F., Macris, N., Miolane, L., and Zdeborová, L. Optimal errors and phase transitions in high-dimensional generalized linear models. *Proceedings of the National Academy of Sciences*, 116(12):5451–5460, 2019.

Barbier, J., Gerace, F., Ingrosso, A., Lauditi, C., Malatesta, E. M., Nwemadji, G., and Ortiz, R. P. Generalization performance of narrow one-hidden layer networks in the teacher-student setting. *arXiv preprint arXiv:2507.00629*, 2025.

Ben Arous, G., Gheissari, R., and Jagannath, A. Online stochastic gradient descent on non-convex losses from high-dimensional inference. *Journal of Machine Learning Research*, 22(106):1–51, 2021.

Bengio, Y., Louradour, J., Collobert, R., and Weston, J. Curriculum learning. In *Proceedings of the 26th annual international conference on machine learning*, pp. 41–48, 2009.

Choromanska, A., Henaff, M., Mathieu, M., Arous, G. B., and LeCun, Y. The loss surfaces of multilayer networks. In *Artificial intelligence and statistics*, pp. 192–204. PMLR, 2015.

Cui, H., Pesce, L., Dandi, Y., Krzakala, F., Lu, Y., Zdeborová, L., and Loureiro, B. Asymptotics of feature learning in two-layer networks after one gradient-step. In Salakhutdinov, R., Kolter, Z., Heller, K., Weller, A., Oliver, N., Scarlett, J., and Berkenkamp, F. (eds.), *Proceedings of the 41st International Conference on Machine Learning*, volume 235 of *Proceedings of Machine Learning Research*, pp. 9662–9695. PMLR, 21–27 Jul 2024.

Damian, A., Lee, J., and Soltanolkotabi, M. Neural networks can learn representations with gradient descent. In *Conference on Learning Theory*, pp. 5413–5452. PMLR, 2022.

Damian, A., Nichani, E., Ge, R., and Lee, J. D. Smoothing the landscape boosts the signal for sgd: Optimal sample complexity for learning single index models. *Advances in Neural Information Processing Systems*, 36:752–784, 2023.

Damian, A., Pillaud-Vivien, L., Lee, J. D., and Bruna, J. Computational-statistical gaps in gaussian single-index models. *arXiv preprint arXiv:2403.05529*, 2024.

Dandi, Y., Krzakala, F., Loureiro, B., Pesce, L., and Stephan, L. How two-layer neural networks learn, one (giant) step at a time. *Journal of Machine Learning Research*, 25(349):1–65, 2024a.

Dandi, Y., Troiani, E., Arnaboldi, L., Pesce, L., Zdeborová, L., and Krzakala, F. The benefits of reusing batches for gradient descent in two-layer networks: Breaking the curse of information and leap exponents. *arXiv preprint arXiv:2402.03220*, 2024b.

Dettmers, T., Pagnoni, A., Holtzman, A., and Zettlemoyer, L. Qlora: Efficient finetuning of quantized llms. *Advances in neural information processing systems*, 36:10088–10115, 2023.

Gardner, E. and Derrida, B. Three unfinished works on the optimal storage capacity of networks. *Journal of Physics A: Mathematical and General*, 22(12):1983, 1989.

Gerace, F., Krzakala, F., Loureiro, B., Stephan, L., and Zdeborová, L. Gaussian universality of perceptrons with random labels. *Physical Review E*, 109(3):034305, 2024.

Goldt, S., Advani, M., Saxe, A. M., Krzakala, F., and Zdeborová, L. Dynamics of stochastic gradient descent for two-layer neural networks in the teacher-student setup. *Advances in neural information processing systems*, 32, 2019.

Goldt, S., Mézard, M., Krzakala, F., and Zdeborová, L. Modeling the influence of data structure on learning in neural networks: The hidden manifold model. *Physical Review X*, 10(4):041044, 2020.

Han, X., Zhang, Z., Ding, N., Gu, Y., Liu, X., Huo, Y., Qiu, J., Yao, Y., Zhang, A., Zhang, L., et al. Pre-trained models: Past, present and future. *Ai Open*, 2:225–250, 2021.

Hayou, S., Ghosh, N., and Yu, B. The impact of initialization on lora finetuning dynamics. *Advances in Neural Information Processing Systems*, 37:117015–117040, 2024.

Houlsby, N., Giurgiu, A., Jastrzebski, S., Morrone, B., De Laroussilhe, Q., Gesmundo, A., Attariyan, M., and Gelly, S. Parameter-efficient transfer learning for nlp. In *International conference on machine learning*, pp. 2790–2799. PMLR, 2019.

Hu, E. J., Shen, Y., Wallis, P., Allen-Zhu, Z., Li, Y., Wang, S., Wang, L., Chen, W., et al. Lora: Low-rank adaptation of large language models. *ICLR*, 1(2):3, 2022.

Isik, B., Ponomareva, N., Hazimeh, H., Paparas, D., Vassilvitskii, S., and Koyejo, S. Scaling laws for downstream task performance in machine translation. In *The Thirteenth International Conference on Learning Representations*, 2025. URL <https://openreview.net/forum?id=vPOMTkmSiu>.

Jang, U., Lee, J. D., and Ryu, E. K. Lora training in the ntk regime has no spurious local minima. *arXiv preprint arXiv:2402.11867*, 2024.

Kalai, A. T. and Sastry, R. The isotron algorithm: High-dimensional isotonic regression. In *COLT*, volume 1, pp. 9, 2009.

Kim, J., Kim, J., and Ryu, E. K. Lora training provably converges to a low-rank global minimum or it fails loudly (but it probably won't fail). *arXiv preprint arXiv:2502.09376*, 2025.

Kratsios, A., Cheng, T. S., Lucchi, A., and Borte, H. S. d. O. Sharp generalization bounds for foundation models with asymmetric randomized low-rank adapters. *arXiv preprint arXiv:2506.14530*, 2025.

Langley, P. Crafting papers on machine learning. In Langley, P. (ed.), *Proceedings of the 17th International Conference on Machine Learning (ICML 2000)*, pp. 1207–1216, Stanford, CA, 2000. Morgan Kaufmann.

Liang, Z., Hu, H., Ye, Q., Xiao, Y., and Li, R. Does low rank adaptation lead to lower robustness against training-time attacks? *arXiv preprint arXiv:2505.12871*, 2025.

Mao, Y., Ge, Y., Fan, Y., Xu, W., Mi, Y., Hu, Z., and Gao, Y. A survey on lora of large language models. *Frontiers of Computer Science*, 19(7):197605, 2025.

Mehta, P., Bukov, M., Wang, C.-H., Day, A. G., Richardson, C., Fisher, C. K., and Schwab, D. J. A high-bias, low-variance introduction to machine learning for physicists. *Physics reports*, 810:1–124, 2019.

Mézard, M., Parisi, G., and Virasoro, M. A. *Spin glass theory and beyond: An Introduction to the Replica Method and Its Applications*, volume 9. World Scientific Publishing Company, 1987.

Mori, F., Mannelli, S. S., and Mignacco, F. Optimal protocols for continual learning via statistical physics and control theory. *Journal of Statistical Mechanics: Theory and Experiment*, 2025(8):084004, 2025.

Mu, S. and Klabjan, D. On the convergence rate of lora gradient descent. *arXiv preprint arXiv:2512.18248*, 2025.

Qiu, X., Sun, T., Xu, Y., Shao, Y., Dai, N., and Huang, X. Pre-trained models for natural language processing: A survey. *Science China technological sciences*, 63(10):1872–1897, 2020.

Robbins, H. and Monro, S. A stochastic approximation method. *The annals of mathematical statistics*, pp. 400–407, 1951.

Saad, D. and Solla, S. Learning with noise and regularizers in multilayer neural networks. *Advances in Neural Information Processing Systems*, 9, 1996.

Saglietti, L., Mannelli, S., and Saxe, A. An analytical theory of curriculum learning in teacher-student networks. *Advances in Neural Information Processing Systems*, 35:21113–21127, 2022.

Sohn, K., Berthelot, D., Carlini, N., Zhang, Z., Zhang, H., Raffel, C. A., Cubuk, E. D., Kurakin, A., and Li, C.-L. Fixmatch: Simplifying semi-supervised learning with consistency and confidence. *Advances in neural information processing systems*, 33:596–608, 2020.

Soletskyi, R., Gabré, M., and Loureiro, B. A theoretical perspective on mode collapse in variational inference. *Machine Learning: Science and Technology*, 6(2):025056, 2025.

Springer, J. M., Goyal, S., Wen, K., Kumar, T., Yue, X., Malladi, S., Neubig, G., and Raghunathan, A. Over-trained language models are harder to fine-tune. In *Forty-second International Conference on Machine Learning*, 2025. URL <https://openreview.net/forum?id=YW6edSufht>.

Veiga, R., Stephan, L., Loureiro, B., Krzakala, F., and Zdeborová, L. Phase diagram of stochastic gradient descent in high-dimensional two-layer neural networks. *Advances in Neural Information Processing Systems*, 35:23244–23255, 2022.

Xu, L., Xie, H., Qin, S.-Z. J., Tao, X., and Wang, F. L. Parameter-efficient fine-tuning methods for pretrained language models: A critical review and assessment. *arXiv preprint arXiv:2312.12148*, 2023.

Xu, Z., Min, H., MacDonald, L. E., Luo, J., Tarmoun, S., Mallada, E., and Vidal, R. Understanding the learning dynamics of lora: A gradient flow perspective on low-rank adaptation in matrix factorization. *arXiv preprint arXiv:2503.06982*, 2025.

Yang, M., Chen, J., Tao, J., Zhang, Y., Liu, J., Zhang, J., Ma, Q., Verma, H., Zhang, R., Zhou, M., et al. Low-rank adaptation for foundation models: A comprehensive review. *arXiv preprint arXiv:2501.00365*, 2024.

Zeng, Y. and Lee, K. The expressive power of low-rank adaptation. *arXiv preprint arXiv:2310.17513*, 2023.

Zhang, Y., Liu, F., and Chen, Y. Lora-one: One-step full gradient could suffice for fine-tuning large language models, provably and efficiently. *arXiv preprint arXiv:2502.01235*, 2025.

A. Recap setting

We are in the following setup:

- **Data:** Data are generated by a noiseless model:

$$y_i = \phi(\omega_* \cdot \mathbf{x}_i), \quad (11)$$

with $\mathbf{x}_i \sim \mathcal{N}(0, I_d)$, $\omega_* \in \mathbb{S}^{d-1}$, and $\phi(x)$ a generic activation function.

- **Model:** We consider the following simplified model for LoRA:

$$\hat{y}_i = f(\mathbf{x}, u, \omega) = \sigma((\tilde{\omega} + u\omega) \cdot \mathbf{x}_i) \quad (12)$$

with

$$\tilde{\omega} = \mu\omega_*, \quad (13)$$

where $\mu \in (0, 1)$; the trainable parameters are $u \in \mathbb{R}$ and $\omega \in \mathbb{S}^{d-1}$.

- **Overlap:** We define the overlaps as follows:

$$m = \omega_* \cdot \omega, \quad m_{\text{eff}} = \mu + um, \quad r = \|\tilde{\omega} + u\omega\|^2 = \mu^2 + u^2 + 2um. \quad (14)$$

An interesting quantity that we can also track is

$$m_{\text{eff}} = \omega_* \cdot (\mu\omega_* + u\omega) = \mu + um, \quad (15)$$

which, in the 1D tensor case, is sufficient to quantify how close the combination $\mu\omega_* + u\omega$ is to ω_* . Notably, at the global minimum—regardless of the activation function or the value of μ —this quantity always equals 1 (or ± 1 for even activations) in the scenario $\phi(\cdot) = \sigma(\cdot)$.

- **Loss:** The population loss under consideration is the mean square loss given by

$$\mathcal{L}(u, \omega) = \frac{1}{2} \mathbb{E}_x \left[(y - \hat{y})^2 \right] = \frac{1}{2} \mathbb{E}_x \left[\left(\phi(\omega_* \cdot \mathbf{x}_i) - \sigma((\mu\omega_* + u\omega) \cdot \mathbf{x}_i) \right)^2 \right], \quad (16)$$

with

$$L(u, \omega) = \frac{1}{2n} \sum_{i=1}^n \left(\phi(\omega_* \cdot \mathbf{x}_i) - \sigma((\mu\omega_* + u\omega) \cdot \mathbf{x}_i) \right)^2$$

being the empirical loss.

We are interested in understanding how the activation functions $\phi(x), \sigma(x)$ and the signal strength μ affect the exit time, namely the time required to exit the search phase. For our analysis, we will consider generic activation functions, for which their Hermite expansions will be exploited subsequently. We investigate correlation-based losses in App. H and show that, for linear activations, pre-trained weights do not affect the dynamics, highlighting that the impact of pre-training depends critically on the choice of loss.

A.1. Another model of pre-training

Another natural candidate for a pre-trained weight is

$$\tilde{\omega} = \mu\omega_* + (1 - \mu)\xi, \quad (17)$$

where ξ is a random unit vector independent of ω_* . In this setting, the effective overlap takes the form

$$m_{\text{eff}} = \mu + (1 - \mu)\omega_* \cdot \xi + um = \mu + um + O(d^{-1/2}), \quad (18)$$

$$r := \|\mu\omega_* + (1 - \mu)\xi + u\omega\|^2 = \mu^2 + (1 - \mu)^2 + u^2 + 2\mu(1 - \mu)\omega_* \cdot \xi + 2\mu um + 2(1 - \mu)u\omega \cdot \xi,$$

$$r = \mu^2 + (1 - \mu)^2 + u^2 + 2\mu um + O(d^{-1/2}), \quad (19)$$

where the $O(d^{-1/2})$ term arises from the high-dimensional limit: with high probability, the dot product of two random vectors is of order $O(d^{-1/2})$, and these vectors therefore remain orthogonal throughout the dynamics.

From (18), we see that, at the level of the overlap m_{eff} , (13) is equivalent to (17). However, the norm of the pre-activation is different from that of (13), as there is an additional $(1 - \mu)^2$ term in this second model (see (14)). Since r^2 also drives the dynamics, computing the gradient with respect to u or m shows that this additional term has no effect on the dynamics of u and m . Therefore, beyond a trivial shift of the pre-activation norm, this model provides no additional insight into the phenomenology observed with (13). We illustrate this by providing in Figure 5, numerical evidence for a student model with pre-trained weights designed according to (17); details of the experimental hyperparameters are provided in the caption. The key takeaway is that the same phenomenology is observed as for the student model (12).

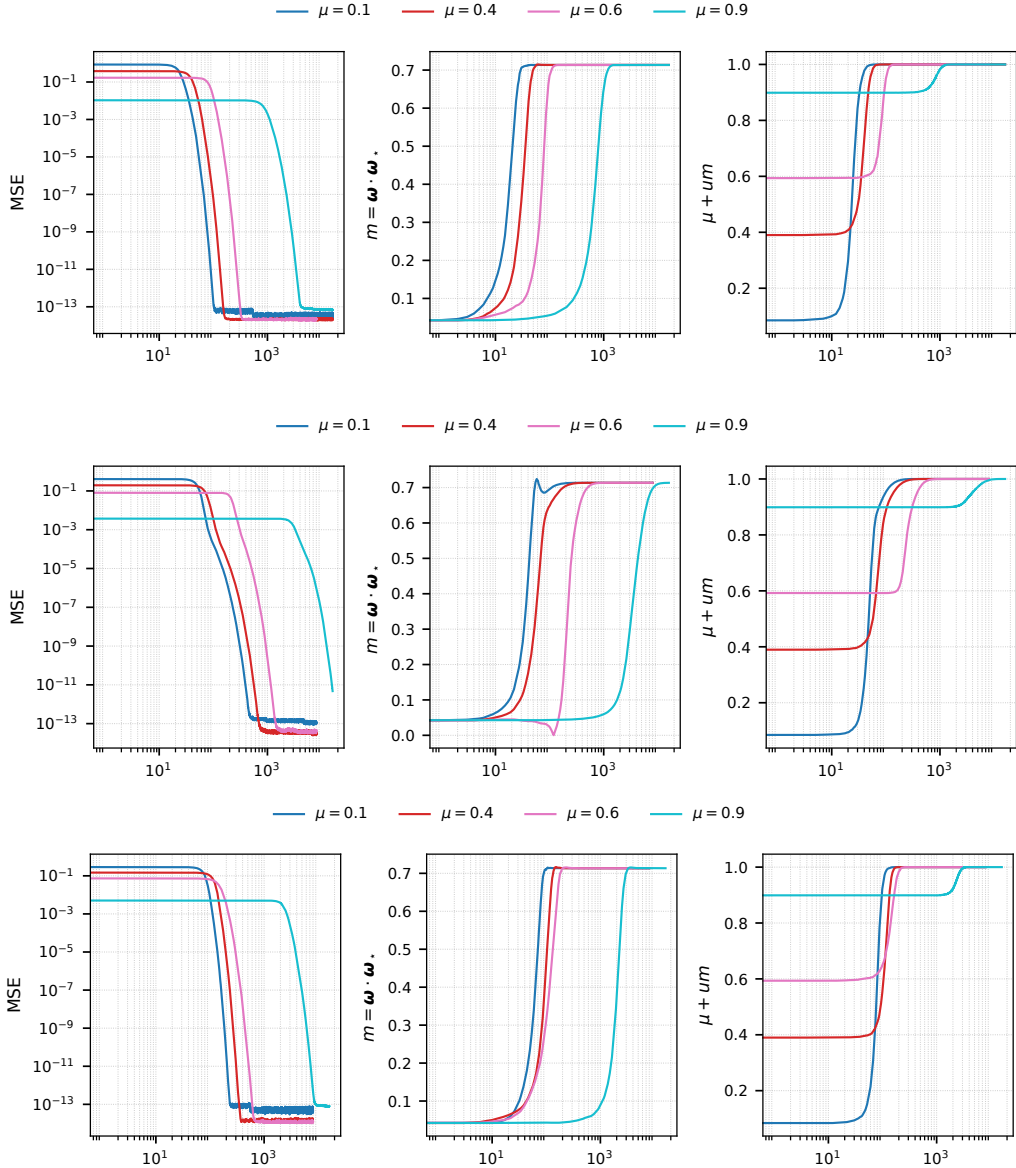


Figure 5. Learning dynamics of the student model (17) for different levels of pre-training alignment $\mu \in \{0.1, 0.4, 0.6, 0.9\}$, trained on data generated by the teacher model (11). We consider the matched teacher–student Linear, Erf, and ReLU (from top to bottom) activation setting and train the student using one-pass SGD with batch size $B = 500$ and input dimension $d = 1000$. The panels report the test mean squared error (MSE) (left), the alignment between the student and teacher directions $m = \omega_* \cdot \omega$ (middle), and the effective teacher–student overlap $m_{\text{eff}} = \mu + um$ (right). Shaded regions indicate one standard deviation over three independent runs. The spherical constraint is enforced by normalizing ω after each gradient step and we used a learning rate $lr = 0.2$.

B. Hermite expansion

B.1. Properties of scaled Hermite polynomials

Let $z \sim \mathcal{N}(0, r)$ with $r > 0$. We denote by $\{\text{He}_k^{[r]}\}_{k \geq 0}$ the probabilists' Hermite polynomials orthogonal with respect to the Gaussian measure $\mathcal{N}(0, r)$.

Definition. The scaled Hermite polynomials are defined through the generating function

$$\exp\left(zt - \frac{rt^2}{2}\right) = \sum_{k=0}^{\infty} \frac{t^k}{k!} \text{He}_k^{[r]}(z). \quad (20)$$

Orthogonality. For all $k, m \geq 0$,

$$\mathbb{E}_{z \sim \mathcal{N}(0, r)} \left[\text{He}_k^{[r]}(z) \text{He}_m^{[r]}(z) \right] = \delta_{km} k! r^k. \quad (21)$$

Zero mean. All non-constant Hermite polynomials have zero expectation:

$$\mathbb{E}_{z \sim \mathcal{N}(0, r)} \left[\text{He}_k^{[r]}(z) \right] = 0 \quad \text{for all } k \geq 1, \quad \text{He}_0^{[r]}(z) = 1. \quad (22)$$

Derivative identity. Hermite polynomials satisfy the lowering relation

$$\frac{d}{dz} \text{He}_k^{[r]}(z) = k \text{He}_{k-1}^{[r]}(z). \quad (23)$$

Multiplication by the coordinate. Multiplication by z raises and lowers the Hermite degree:

$$z \text{He}_k^{[r]}(z) = \text{He}_{k+1}^{[r]}(z) + k r \text{He}_{k-1}^{[r]}(z). \quad (24)$$

Scaling relation. If $z = \sqrt{r} x$ with $x \sim \mathcal{N}(0, 1)$, then

$$\text{He}_k^{[r]}(z) = r^{k/2} \text{He}_k(x), \quad (25)$$

where He_k denotes the standard probabilists' Hermite polynomial.

Ornstein–Uhlenbeck eigenfunctions. Define the Ornstein–Uhlenbeck operator

$$\mathcal{L}_r f(z) := r f''(z) - z f'(z). \quad (26)$$

Then Hermite polynomials are eigenfunctions of \mathcal{L}_r :

$$\mathcal{L}_r \text{He}_\ell^{[r]}(z) = -\ell \text{He}_\ell^{[r]}(z). \quad (27)$$

Parity. Hermite polynomials have definite parity:

$$\text{He}_\ell^{[r]}(-z) = (-1)^\ell \text{He}_\ell^{[r]}(z). \quad (28)$$

As a consequence, even (resp. odd) functions have vanishing odd (resp. even) Hermite coefficients.

Hermite expansion of square-integrable functions. Any function $\sigma \in L^2(\mathcal{N}(0, r))$ admits the expansion

$$\sigma(z) = \sum_{k=0}^{\infty} \frac{\sigma_k^{[r]}}{k! r^k} \text{He}_k^{[r]}(z), \quad \sigma_k^{[r]} := \mathbb{E} \left[\sigma(z) \text{He}_k^{[r]}(z) \right]. \quad (29)$$

Gaussian expectation. Only the zeroth Hermite coefficient contributes to the mean:

$$\mathbb{E}_{z \sim \mathcal{N}(0, r)}[\sigma(z)] = \sigma_0^{[r]}. \quad (30)$$

Interpretation. The family $\{\text{He}_\ell^{[r]}\}_{\ell \geq 0}$ forms an orthogonal basis of $L^2(\mathcal{N}(0, r))$, often referred to as the Wiener chaos decomposition. Each Hermite degree corresponds to an independent mode under Gaussian expectations and dynamics.

B.2. Hermite expansion of a generic activation function

The Hermite expansion of $\phi(\cdot)$ with preactivation $z \sim \mathcal{N}(0, 1)$ is

$$\phi(z) = \sum_{k \geq 0} \frac{\phi_k}{k!} \text{He}_k(z) \quad \Rightarrow \quad \mathbb{E}[\phi(z)^2] = \int Dz \phi(z)^2 = \sum_{k=0}^{\infty} \frac{\phi_k^2}{k!}, \quad (31)$$

with

$$Dz := dz \exp(-z^2/2)/\sqrt{2\pi}.$$

Now consider $z_1 \sim \mathcal{N}(0, r_1)$ and $z_2 \sim \mathcal{N}(0, r_2)$. From the Mehler expansion, one gets

$$\mathbb{E}[\sigma(z_1)\sigma(z_2)] = \sum_{k=0}^{\infty} \frac{\sigma_k^{[r_1]}\sigma_k^{[r_2]}}{k! r_1^k r_2^k} h^k, \quad \text{with} \quad h = \mathbb{E}[z_1 z_2]. \quad (32)$$

As a warm-up, let us compute how the population loss depends on the summary statistic m :

$$\mathcal{L}(\omega) = \frac{1}{2} \mathbb{E}[(\phi(\omega_\star \cdot x) - \sigma((\mu\omega_\star + u\omega) \cdot x))^2] = \frac{1}{2} (\mathbb{E}[\phi(\lambda_\star)^2] + \mathbb{E}[\sigma(\mu\lambda_\star + u\lambda)^2] - \mathbb{E}[\phi(\lambda_\star)\sigma(\mu\lambda_\star + u\lambda)]), \quad (33)$$

where we recall $\lambda_\star = \omega_\star \cdot x$ and $\lambda = \omega \cdot x$.

Now let us recall the distribution of the different preactivations:

$$\lambda_\star \sim \mathcal{N}(0, 1), \quad \mu\lambda_\star + u\lambda \sim \mathcal{N}(0, r), \quad \mathbb{E}[\lambda_\star(\mu\lambda_\star + u\lambda)] = \mu + um,$$

with $m = \omega_\star \cdot \omega$ and $r = \mu^2 + u^2 + 2\mu um$.

One then exploits the previous property to obtain

$$\begin{aligned} \mathbb{E}[\phi(\lambda_\star)^2] &= \sum_{k=0}^{+\infty} \frac{\phi_k^2}{k!}, \\ \mathbb{E}[\sigma(\mu\lambda_\star + u\lambda)^2] &= \sum_{k=0}^{+\infty} \frac{(\sigma_k^{[r]})^2}{k! r^k}, \\ \mathbb{E}[\phi(\lambda_\star)\sigma(\mu\lambda_\star + u\lambda)] &= \sum_{k=0}^{+\infty} \frac{\phi_k \sigma_k^{[r]}}{k! r^k} (\mu + um)^k. \end{aligned}$$

The population loss becomes

$$\mathcal{L}(u, m) = \sum_{k=0}^{+\infty} \frac{\phi_k^2}{2k!} + \sum_{k=0}^{+\infty} \frac{(\sigma_k^{[r]})^2}{2k! r^k} - \sum_{k=0}^{+\infty} \frac{\sigma_k^{[r]}\phi_k}{k! r^k} (\mu + um)^k = \sum_{k=0}^{+\infty} \frac{\phi_k^2}{2k!} + \mathcal{L}_1(u, m) + \mathcal{L}_2(u, m). \quad (34)$$

B.3. Expansion for non-unit variance pre-activation in the standard Hermite basis

In Appendix B.2, we derived in (29) the Hermite expansion of an activation function under a Gaussian pre-activation with zero mean and non-unit variance, expressed in the Hermite basis associated with the corresponding Gaussian measure. Since the information exponent (IE) is defined with respect to the standard Hermite basis associated with a unit-variance

Gaussian (Ben Arous et al., 2021), our goal in this appendix is to map the resulting expansion onto the standard Hermite basis.

Using the definition of Hermite polynomials associated with a Gaussian measure of variance r (see (20)), we can rewrite (25) as

$$\text{He}_k^{[r]}(z) = r^{k/2} \text{He}_k\left(\frac{z}{\sqrt{r}}\right),$$

which follows from the change of variables $t \mapsto t/\sqrt{r}$ in the generating function. To express this polynomial in the standard Hermite basis, we use the classical Hermite scaling identity

$$\text{He}_k(az) = \sum_{j=0}^{\lfloor k/2 \rfloor} a^{k-2j} (a^2 - 1)^j \frac{k!}{(k-2j)! j! 2^j} \text{He}_{k-2j}(z).$$

Applying this identity with $a = 1/\sqrt{r}$, we obtain $a^{k-2j} = r^{-(k-2j)/2}$ and $a^2 - 1 = (1-r)/r$. Multiplying by the prefactor $r^{k/2}$ yields

$$r^{k/2} a^{k-2j} (a^2 - 1)^j = (-1)^j (r-1)^j,$$

which leads to the expansion

$$\text{He}_k^{[r]}(z) = \sum_{j=0}^{\lfloor k/2 \rfloor} (-1)^j (r-1)^j \frac{k!}{(k-2j)! j! 2^j} \text{He}_{k-2j}(z). \quad (35)$$

This expression shows that if the coefficients of the non-standard expansion satisfy $\sigma_k^{[r]} = 0$ for all $k \leq k^* - 1$, with $\sigma_{k^*}^{[r]} \neq 0$, then the lowest-order Hermite polynomial appearing in the standard basis expansion is either He_0 or He_1 , depending on the parity of k^* . As a consequence, the information exponent of the resulting activation function is at most 2, independently of the choice of activation.

Finally, expressing the non-unit-variance expansion (29) in the standard Hermite basis yields

$$\sigma(z) = \sum_{k \geq 0} \frac{\sigma_k^{[r]}}{k! r^k} \sum_{j=0}^{\lfloor k/2 \rfloor} (-1)^j (r-1)^j \frac{k!}{(k-2j)! j! 2^j} \text{He}_{k-2j}(z). \quad (36)$$

B.4. Squaring a Hermite activation

We argued in the main text that squaring the labels constitutes a natural transformation that can reduce the information exponent (IE) of an activation function. In this appendix, we provide the mathematical justification for this claim. Since the student activation function has IE at most 2, it suffices to apply such a transformation to the teacher activation only.

Starting from the Hermite expansion for unit-variance pre-activations (31), we write

$$(\sigma(z))^2 = \sum_{k, k' \geq 0} \frac{\sigma_k \sigma_{k'}}{k! k'!} \text{He}_k(z) \text{He}_{k'}(z) = \sum_{k, k' \geq 0} \frac{\sigma_k \sigma_{k'}}{k! k'!} \sum_{j=0}^{\min(k, k')} j! \binom{k}{j} \binom{k'}{j} \text{He}_{k+k'-2j}(z). \quad (37)$$

We now specialize to the case where the activation is a pure Hermite polynomial, $\sigma(z) = \text{He}_k(z)$. In this case, the above expression reduces to

$$(\sigma(z))^2 = \sum_{j=0}^k j! \binom{k}{j}^2 \text{He}_{2k-2j}(z) = k! \text{He}_0(z) + k^2 (k-1)! \text{He}_2(z) + \dots \quad (38)$$

The expansion (38) shows that, besides the constant term, the lowest-order Hermite polynomial appearing in $(\sigma(z))^2$ is $\text{He}_2(z)$. Since the constant component does not affect correlations with the input direction, the effective lowest non-trivial Hermite level governing the learning dynamics is therefore He_2 . As a consequence, squaring a pure Hermite activation reduces the information exponent of the teacher to $\text{IE} = 2$, independently of the original degree k .

Eliminating the delay near the singularity with two stage learning based on label transformation In the main, we showed that label transformations can enable the student to learn faster by effectively reducing the escape time from the correlated search phase. Focusing on label squaring, we demonstrated that this transformation can eliminate the singularity that arises for certain activation functions. In Figure 6, we provide numerical evidence for a two-stage learning procedure at a pre-training alignment $\mu = 0.325$, which was shown to correspond to a near-singular regime (i.e., failure to escape the correlated search phase cf. Figure 3) for the Hermite-3 activation He_3 . Across both stages, the student is trained using one-pass SGD (details of the experimental setup are provided in the caption). The two stages differ as follows: in the first stage, the labels are squared and used to train the student; once training has proceeded for a sufficiently long time, we revert to the original labels in the second stage. As observed in Figure 6, this learning paradigm enables a much faster escape from the correlated search phase—compared to the standard training procedure shown in Figure 12—and subsequently allows the student to recover the teacher direction during the descent phase.

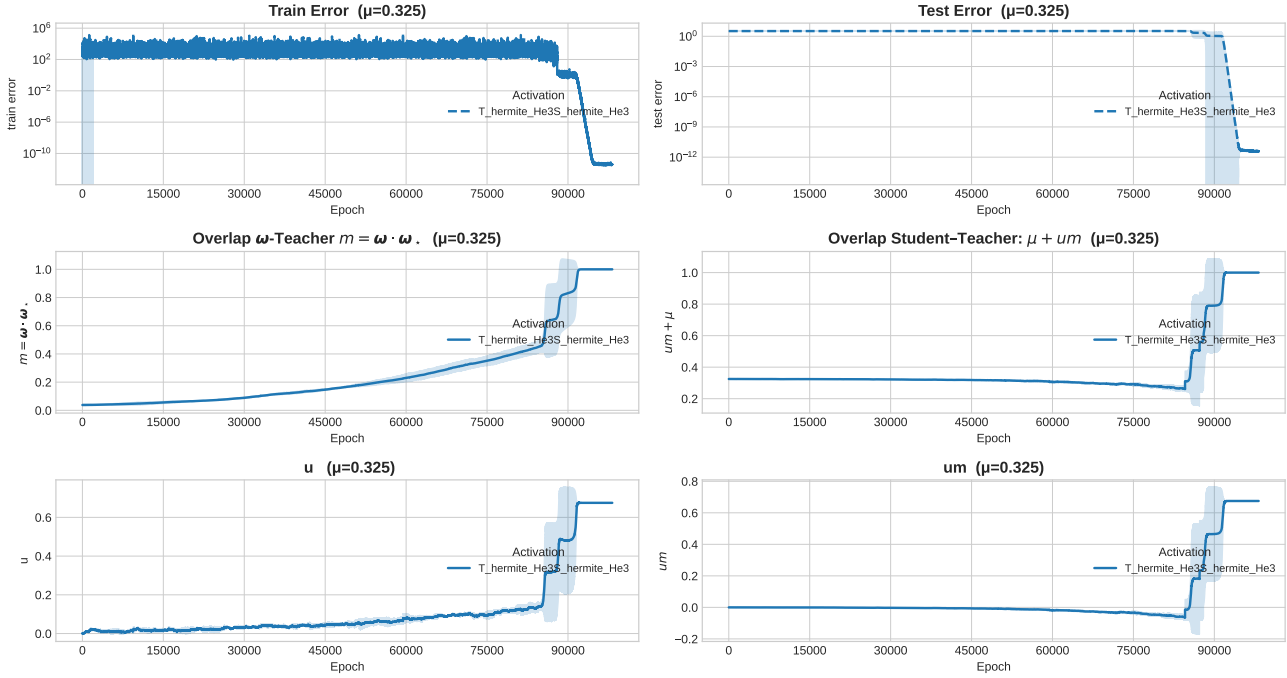


Figure 6. Learning dynamics of the student model (12) for a pre-training alignment level $\mu = 0.325$, trained on data generated by the teacher model (11). Both teacher and student activations are Hermite polynomials of degree $k = 3$, as indicated in the legend. The student is trained using a two-stage one-pass SGD procedure. In the first stage, the ground-truth labels are squared and used until the overlap m converges to approximately 0.5; in the second stage, training proceeds using the original labels. The hyperparameters are a batch size $B = 1000$ and input dimension $d = 1000$. A spherical constraint is enforced by normalizing ω after each gradient step, and the learning rate is set to $lr = 10^{-2} \delta_k$, with $\delta_k = 1/(k! k)$. We note that when standard one-pass SGD is used on square label, the overlap remains close to zero ($m \simeq 0.04$; see the third row of Fig. 12) even after 2.5×10^5 epochs. In contrast, with the two-stage procedure, the overlap has already escaped the correlated search phase by 2×10^4 epochs. The first stage ends at approximately 8.5×10^4 epochs; during the second stage, a long plateau is observed before the dynamics eventually converge toward the global minimum of the loss. Results are averaged over three independent runs. The observed staircase-like behavior arises from averaging across different random seeds: when the second learning phase begins, each seed reaches global convergence at a slightly different epoch. Because the transition is sharp, averaging these misaligned jumps produces the apparent stepwise structure.

C. Spherical gradient flow equation

We consider the spherical variant of stochastic gradient descent (SGD), where the weight vector $\omega \in \mathbb{S}^{d-1}$ is constrained to lie on the unit sphere. The update rule reads

$$\omega^{t+1} = \frac{\omega^t - \gamma \nabla_{\omega}^{\mathbb{S}^{d-1}} \mathcal{L}(u, \omega)}{\|\omega^t - \gamma \nabla_{\omega}^{\mathbb{S}^{d-1}} \mathcal{L}(u, \omega)\|}, \quad (39)$$

where $\nabla_{\omega}^{\mathbb{S}^{d-1}}$ denotes the spherical gradient. Explicitly, it is given by

$$\mathbf{h} := \nabla_{\omega}^{\mathbb{S}^{d-1}} \mathcal{L}(u, \omega) = (I_d - \omega \omega^T) \nabla_{\omega} \mathcal{L}(u, \omega) = (\omega_{\star} - m \omega) \frac{\partial \mathcal{L}}{\partial m}, \quad (40)$$

where $m = \omega \cdot \omega_{\star}$. In the last equality, we used the decomposition

$$\nabla_{\omega} \mathcal{L}(u, \omega) = 2\omega \frac{\partial \mathcal{L}}{\partial q} + \omega_{\star} \frac{\partial \mathcal{L}}{\partial m}. \quad (41)$$

Small learning-rate expansion. Assuming γ to be small, we expand the normalization factor in (39):

$$\|\omega^t - \gamma \mathbf{h}\|^{-1} = \left(1 + \gamma^2 \|\mathbf{h}\|^2\right)^{-1/2} = 1 - \frac{\gamma^2}{2} \|\mathbf{h}\|^2 + O(\gamma^3), \quad (42)$$

where

$$\|\mathbf{h}\|^2 = (1 - m^2) \left(\frac{\partial \mathcal{L}}{\partial m}\right)^2. \quad (43)$$

Evolution of the overlap. Multiplying (39) by ω_{\star} yields the update equation for the overlap:

$$\begin{aligned} m^t &= \left(m^{t-1} - \gamma \mathbf{h} \cdot \omega_{\star}\right) \left(1 - \frac{\gamma^2}{2} \|\mathbf{h}\|^2 + O(\gamma^3)\right) \\ &= m^{t-1} - \gamma \left(\mathbf{h} \cdot \omega_{\star} - \frac{\gamma}{2} \|\mathbf{h}\|^2 m^{t-1}\right) + O(\gamma^3), \end{aligned} \quad (44)$$

with

$$\mathbf{h} \cdot \omega_{\star} = (1 - m^2) \frac{\partial \mathcal{L}}{\partial m}. \quad (45)$$

The update is contractive provided the learning rate satisfies

$$\gamma \leq \frac{2 \mathbf{h} \cdot \omega_{\star}}{\|\mathbf{h}\|^2 m} \iff \gamma \leq \frac{2}{m} \left(\frac{\partial \mathcal{L}}{\partial m}\right)^{-1}. \quad (46)$$

Continuous-time limit. We now set $\gamma = \delta dt$ with $\delta \in \mathbb{R}$ chosen such that the stability condition (46) holds. Equation (44) then becomes

$$\frac{m^t - m^{t-1}}{dt} = -\delta \mathbf{h} \cdot \omega_{\star} + O(\delta^2 dt^2). \quad (47)$$

Taking the limit $dt \rightarrow 0$ yields the gradient-flow equation

$$\frac{dm}{dt} = -\delta(1 - m^2) \frac{\partial \mathcal{L}}{\partial m}. \quad (48)$$

Similarly, differentiation with respect to u gives

$$\frac{du}{dt} = -\delta \frac{\partial \mathcal{L}}{\partial u}. \quad (49)$$

Choice of time rescaling. The parameter δ is introduced to ensure that the dynamical equations (48)–(49) remain $\mathcal{O}(1)$ for different choices of activation functions, which affect the scaling of $\partial \mathcal{L} / \partial m$ and $\partial \mathcal{L} / \partial u$. In particular, for pure Hermite activations of degree k^* , an appropriate choice is

$$\delta = (k^*! k^*)^{-1}. \quad (50)$$

D. Population loss analysis

D.1. Gradient of the population loss

By leveraging (29) and (31), the population loss defined in (33) becomes:

$$\mathcal{L}(u, m) = \sum_{k=0}^{+\infty} \frac{\phi_k^2}{2k!} + \sum_{k=0}^{+\infty} \frac{(\sigma_k^{[r]})^2}{2k!r^k} - \sum_{k=0}^{+\infty} \frac{\sigma_k^{[r]}\phi_k}{k!r^k}(\mu + um)^k$$

with $m = \omega_* \cdot \omega$, $r = \mu^2 + u^2 + 2\mu um$.

The partial derivative of \mathcal{L} respect to u and m are

$$\begin{aligned} \frac{\partial \mathcal{L}}{\partial u} &= (u + \mu m) \sum_{k=0}^{+\infty} \frac{\sigma_k^{[r]}\bar{\sigma}_k^{[r]}}{k!r^{k+1}} - \sum_{k=0}^{+\infty} \phi_k(\mu + um)^{k-1} \left[-\frac{(u + m\mu)(\mu + mu)}{(k-1)!r^{k+1}}\sigma_k^{[r]} + \frac{\sigma_k^{[r]}m}{(k-1)!r^k} + \frac{(\mu + mu)(u + m\mu)\bar{\sigma}_k^{[r]}}{k!r^{k+1}} \right] \\ \frac{\partial \mathcal{L}}{\partial m} &= u\mu \sum_{k=0}^{+\infty} \frac{\sigma_k^{[r]}\bar{\sigma}_k^{[r]}}{k!r^{k+1}} - \sum_{k=0}^{+\infty} \phi_k(\mu + um)^{k-1} \left[-\frac{u\mu(\mu + mu)}{(k-1)!r^{k+1}}\sigma_k^{[r]} + \frac{u\sigma_k^{[r]}}{(k-1)!r^k} + \frac{(\mu + mu)u\mu\bar{\sigma}_k^{[r]}}{k!r^{k+1}} \right] \end{aligned} \quad (51)$$

with $\bar{\sigma}_k^{[r]} = r^{\frac{k+1}{2}} \int Dz \text{He}_k(z) \sigma'(z\sqrt{r})z$. The summation $\sum_{k=0}^{+\infty}$ is used in a loose manner to lighten the notation. It should be understood that whenever a factorial prefactor of the form $1/(k-1)!$ appears, the summation effectively starts at $k=1$ rather than $k=0$.

D.2. Gradient of the population loss in the correlated search phase

In this phase we are using $m \ll \mu$ and $u \ll \mu$, we can then do the following simplification $\mu + um \simeq \mu$, $r \simeq \mu^2$, (51) becomes

$$\begin{aligned} \frac{\partial \mathcal{L}}{\partial u} &= m \sum_{k=0}^{+\infty} \frac{\bar{\sigma}_k^{[r]}}{k!\mu^{k+1}} \left(-\phi_k + \frac{\sigma_k^{[r]}}{\mu^k} \right) + u \sum_{k=0}^{+\infty} \left[\frac{\bar{\sigma}_k^{[r]}\sigma_k^{[r]}}{k!r^{k+1}} + \frac{\phi_k}{(k-1)!\mu^{k+2}} \left(\sigma_k^{[r]} - \frac{\bar{\sigma}_k^{[r]}}{k} \right) \right] \\ \frac{\partial \mathcal{L}}{\partial m} &= u \sum_{k=0}^{+\infty} \frac{\bar{\sigma}_k^{[r]}}{k!\mu^{k+1}} \left(-\phi_k + \frac{\sigma_k^{[r]}}{\mu^k} \right), \end{aligned} \quad (52)$$

where $\sigma_k^{[r]}$ and $\bar{\sigma}_k^{[r]}$ can be rewritten to become

$$\sigma_k^{[r]} = r^{\frac{k}{2}} \int Dz \text{He}_k(z) \sigma(z\sqrt{r}) = r^{\frac{k}{2}} \mathbb{E}[\text{He}_k(z) \sigma(z\sqrt{r})], \quad \bar{\sigma}_k^{[r]} = r^{\frac{k+1}{2}} \int Dz \text{He}_k(z) z \sigma'(z\sqrt{r}) = r^{\frac{k+1}{2}} \mathbb{E}[z \text{He}_k(z) \sigma'(z\sqrt{r})]. \quad (53)$$

The equations (52) can be cast as

$$\frac{\partial \mathcal{L}}{\partial u} = -uB - mA \quad (54)$$

$$\frac{\partial \mathcal{L}}{\partial m} = -uA \quad (55)$$

with

$$A = - \sum_{k=0}^{+\infty} \frac{\bar{\sigma}_k^{[r]}}{k!\mu^{k+1}} \left(-\phi_k + \frac{\sigma_k^{[r]}}{\mu^k} \right), \quad B = - \sum_{k=0}^{+\infty} \left[\frac{\bar{\sigma}_k^{[r]}\sigma_k^{[r]}}{k!\mu^{2k+2}} + \frac{\phi_k}{(k-1)!\mu^{k+2}} \left(\sigma_k^{[r]} - \frac{\bar{\sigma}_k^{[r]}}{k} \right) \right]. \quad (56)$$

E. Escaping the correlated search phase

E.1. Generic activation function: proof of Prop. 1

Proof. Using (48) and (49), together with the linearized gradients (54) and (55), one obtains

$$\begin{cases} \frac{du}{dt} = uB + mA, \\ \frac{dm}{dt} = uA, \end{cases} \quad (57)$$

where the factor δ has been absorbed into the definitions of A and B .

We rewrite (57) in matrix form as

$$\begin{bmatrix} \dot{u} \\ \dot{m} \end{bmatrix} = \begin{bmatrix} B & A \\ A & 0 \end{bmatrix} \begin{bmatrix} u \\ m \end{bmatrix}. \quad (58)$$

This matrix has eigenvalues

$$\lambda_{\pm}(\mu) = \frac{B \pm \sqrt{B^2 + 4A^2}}{2}. \quad (59)$$

In the correlated search regime of interest, we assume $A \neq 0$, so that $\lambda_+(\mu) > 0$ and the fixed point is linearly unstable.

Let $\epsilon := u_0^2 + m_0^2$ denote the squared norm of the initial condition. Solving the linear system yields exponential growth along the unstable eigendirection at rate $\lambda_+(\mu)$. As a result, the exit time from a ball of radius R satisfies, up to additive constants,

$$t_{\text{exit}}(\mu) = \frac{1}{\lambda_+(\mu)} \log\left(\frac{R}{\sqrt{\epsilon}}\right) + \mathcal{O}(1). \quad (60)$$

We now specify the initialization. For random isotropic initialization on the sphere, we have $m_0 = \mathcal{O}(d^{-1/2})$ with high probability. We further assume $u_0^2 \sim m_0^2$, so that $\epsilon \sim d^{-1}$. For any fixed escape radius $R > 0$, this yields

$$t_{\text{exit}}(\mu) = \frac{1}{2\lambda_+(\mu)} \log d + \mathcal{O}(1). \quad (61)$$

Recalling that $\tau(\mu) = \lambda_+(\mu)^{-1}$, we conclude that

$$t_{\text{exit}} \sim \frac{\tau(\mu)}{2} \log d, \quad (62)$$

which proves Prop. 1. \square

E.2. Case of linear activation function

The dynamics of the order parameters are given by

$$\begin{cases} \dot{u} = (1 - \mu)m - u, \\ \dot{m} = (1 - \mu)u(1 - m^2). \end{cases}$$

Linearizing the dynamics around the fixed point $(u, m) = (0, 0)$ yields a linear system whose Jacobian matrix has eigenvalues

$$\lambda_{\pm}(\mu) = \frac{-1 \pm \sqrt{1 + 4(1 - \mu)^2}}{2}.$$

The associated characteristic time scale $\tau(\mu)$ is given by

$$\tau(\mu) = \frac{1}{\lambda_+(\mu)} = \frac{1 + \sqrt{1 + 4(1 - \mu)^2}}{2(1 - \mu)^2}.$$

Note that this time scale diverges as $\mu \rightarrow 1^-$:

$$\tau(\mu) \sim \frac{1}{(1 - \mu)^2}, \quad \text{as } \mu \rightarrow 1^-.$$

E.3. Numerical evidence for function with $\text{IE} = 1$

Figure 7 provides additional evidence of catastrophic overtraining across linear, erf, ReLU, and sigmoid activations over a wide range of pre-training alignments, with experimental details given in the caption.

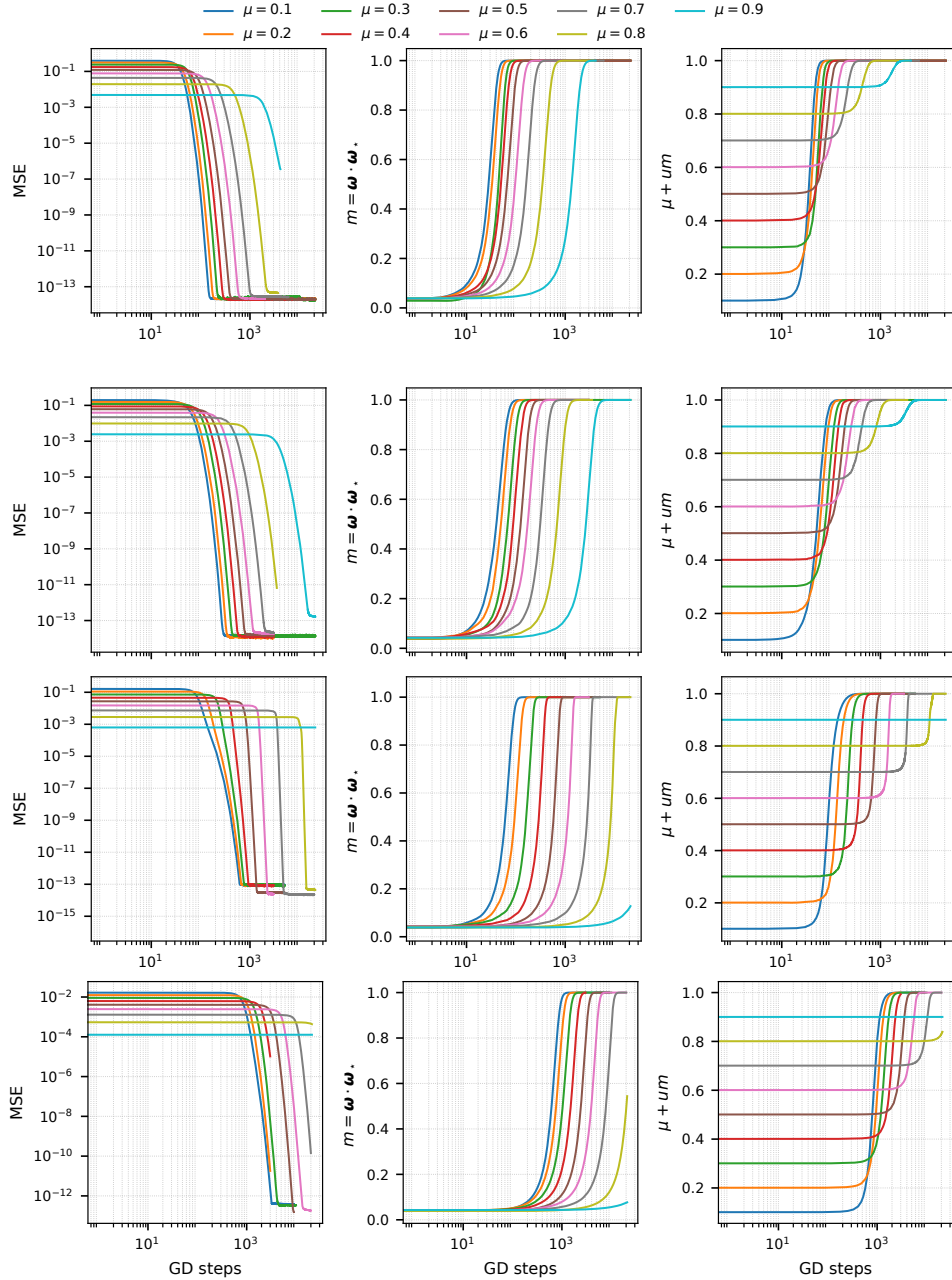


Figure 7. Learning dynamics of the student model (12) for different levels of pre-training alignment $\mu \in \{0.1, 0.2, 0.3, 0.4, 0.5, 0.8, 0.9\}$, trained on data generated by the teacher model (11). We consider the matched teacher–student Linear, ReLU, Erf, and Sigmoid (from top to bottom) activation setting and train the student using one-pass SGD with batch size $B = 500$ and input dimension $d = 1000$. The panels report the test mean squared error (MSE) (left), the alignment between the student and teacher directions $m = \omega_\star \cdot \omega$ (middle), and the effective teacher–student overlap $m_{\text{eff}} = \mu + um$ (right). Shaded regions indicate one standard deviation over three independent runs. The spherical constraint is enforced by normalizing ω after each gradient step and we used a learning rate $lr = 0.2$.

E.4. Case of pure Hermite polynomial: proof of Propositions 2 and 3

A common ingredient in these propositions is that they all involve the quantities A and B . We therefore first derive explicit analytical expressions for these quantities in the case of Hermite polynomial activations, and then use these expressions to complete the proofs of each result. For this class of functions, the Hermite coefficients $\sigma_k^{[r]}$ can be computed explicitly.

Assume that $\sigma(\cdot)$ is the k^* -th Hermite polynomial. This implies that $\sigma_k = \sigma_{k^*} \delta_{k^*,k} = k^*! \delta_{k^*,k}$. The associated Hermite expansion for the student in the standard Hermite basis then reads:

$$\sigma_k = \sigma_{k^*} \delta_{k^*,k} = k^*! \delta_{k^*,k}, \quad \sigma_k^{[r]} = r^{\frac{k}{2}} \mathbb{E}[\text{He}_k(z) \text{He}_{k^*}(z\sqrt{r})], \quad \bar{\sigma}_k^{[r]} = r^{\frac{k}{2}} \mathbb{E}[\text{He}_k(z) z\sqrt{r} \text{He}_{k^*}'(z\sqrt{r})]. \quad (63)$$

By leveragint the following property

$$\begin{aligned} \mathbb{E}[\text{He}_i(z) \text{He}_j(az)] &= \begin{cases} j! a^i \frac{\left(\frac{a^2-1}{2}\right)^{\frac{j-i}{2}}}{\left(\frac{j-i}{2}\right)!}, & \text{if } j \geq i \text{ and } j-i = 2h, \\ 0 & \text{otherwise,} \end{cases} \\ \text{He}_k'(x) &= k \text{He}_{k-1}(x) \\ x \text{He}_k'(x) &= kx \text{He}_{k-1}(x) = k \left(\text{He}_k(x) + (k-1) \text{He}_{k-2}(x) \right) \end{aligned}$$

we obtain the following coefficient

$$\sigma_k = \sigma_{k^*} \delta_{k^*,k} = k^*! \delta_{k^*,k}, \quad \sigma_k^{[r]} = k^*! r^k \frac{\left(\frac{r-1}{2}\right)^{\frac{k^*-k}{2}}}{\left(\frac{k^*-k}{2}\right)!} \text{ for which } 0 \leq k \leq k^* \text{ and } k \equiv k^* \pmod{2}. \quad (64)$$

$$\bar{\sigma}_k^{[r]} = \begin{cases} k^*! r^k \frac{\left(\frac{r-1}{2}\right)^{\frac{k^*-2-k}{2}}}{\left(\frac{k^*-2-k}{2}\right)!} \binom{k^*r-k}{k^*-k}, & \text{if } 0 \leq k < k^* \text{ and } k \equiv k^* \pmod{2} \\ k^* \sigma_k^{[r]} & \text{if } k = k^*. \end{cases}$$

For $k = k^*$ the coefficient blend to

$$\sigma_{k^*}^{[r]} = k^*! r^{k^*}, \quad \bar{\sigma}_{k^*}^{[r]} = k^*! k^* r^{k^*}.$$

In the next we define the admissible indices k as integers satisfying $0 \leq k < k^*$ and $k \equiv k^* \pmod{2}$, we will plug-in these expressions into A and B (see (56)) that leads to

$$\begin{aligned} A &= - \left[\frac{k^*! k^* r^{k^*}}{k^*! \mu^{k^*+1}} (-k^*! + \frac{k^*! r^{k^*}}{\mu^{k^*}}) + \sum_{k < k^*} \frac{\bar{\sigma}_k^{[r]} \sigma_k^{[r]}}{k! \mu^{2k+1}} \right] = - \left[k^*! k^* \mu^{k^*-1} (-1 + \mu^{k^*}) + \sum_{k < k^*} \frac{\bar{\sigma}_k^{[r]} \sigma_k^{[r]}}{k! \mu^{2k+1}} \right] \\ B &= - \left[\frac{(k^*!)^2 k^* r^{2k^*}}{k^*! \mu^{2k^*+2}} + \sum_{k < k^*} \frac{\bar{\sigma}_k^{[r]} \sigma_k^{[r]}}{k! \mu^{2k+2}} \right] = - \left[k^*! k^* \mu^{2k^*-2} + \sum_{k < k^*} \frac{\bar{\sigma}_k^{[r]} \sigma_k^{[r]}}{k! \mu^{2k+2}} \right] \end{aligned} \quad (65)$$

with

$$\bar{\sigma}_k^{[r]} \sigma_k^{[r]} = (k^*!)^2 r^{2k} \frac{\left(\frac{r-1}{2}\right)^{k^*-k-1}}{\left(\frac{k^*-k}{2}\right)! \left(\frac{k^*-k-2}{2}\right)!} \binom{k^*r-k}{k^*-k} \Rightarrow \frac{\bar{\sigma}_k^{[r]} \sigma_k^{[r]}}{k! \mu^{2k}} = \frac{(k^*!)^2}{k!} \mu^{2k} \frac{\left(\frac{r-1}{2}\right)^{k^*-k-1}}{\left(\frac{k^*-k}{2}\right)! \left(\frac{k^*-k-2}{2}\right)!} \binom{k^*r-k}{k^*-k},$$

that becomes

$$\frac{\bar{\sigma}_k^{[r]} \sigma_k^{[r]}}{k! \mu^{2k+2}} = \frac{(k^*!)^2}{k!} \mu^{2k-2} \frac{\left(\frac{r-1}{2}\right)^{k^*-k-1}}{\left(\frac{k^*-k}{2}\right)! \left(\frac{k^*-k-2}{2}\right)!} \binom{k^*r-k}{k^*-k}. \quad (66)$$

Using (66), (65) becomes

$$A = - \left[k^*!k^* \mu^{k^*-1} (-1 + \mu^{k^*}) + (k^*!)^2 \mu^{-1} f(k^*, \mu) \right], \quad B = - \left[k^*!k^* \mu^{2k^*-2} + (k^*!)^2 \mu^{-2} f(k^*, \mu) \right], \quad (67)$$

which after rescaling $A \rightarrow \frac{A}{k^*!k^*}$ and $B \rightarrow \frac{B}{k^*!k^*}$ (we set $\delta = (k^*!k^*)^{-1}$ as it was mentioned in (50)) becomes

$$A = - \left[\mu^{k^*-1} (-1 + \mu^{k^*}) + \frac{(k^*!)^2}{k^*} \mu^{-1} f(k^*, \mu) \right], \quad \text{and} \quad B = - \left[\mu^{2k^*-2} + \frac{k^*!}{k^*} \mu^{-2} f(k^*, \mu) \right], \quad (68)$$

with f given by

$$f(k^*, \mu) = \sum_{k < k^*} \frac{\mu^{2k}}{k!} \frac{\left(\frac{r-1}{2}\right)^{k^*-k-1}}{\left(\frac{k^*-k}{2}\right)! \left(\frac{k^*-k-2}{2}\right)!} \binom{k^*r-k}{k^*-k} = \sum_{m=1}^p \frac{\left(1 + \frac{k^*(r-1)}{2m}\right) \mu^{2(k^*-2m)} (r-1)^{2m-1}}{(k^*-2m)!m!(m-1)!2^{2m-1}}, \quad (69)$$

where $m = \frac{k^*-k}{2}$ and we assume $k^* = 2p+1$ or $k^* = 2p$.

Now we are concerned with values of μ in the neighborhood of zero such that the lowest power of μ dominates $f(k^*, \mu)$. Since $r = \mu^2$ then

$$\left(1 + \frac{k^*(r-1)}{2m}\right) = 1 - \frac{k^*}{2m} + \frac{k^*}{2m}\mu^2$$

$$(r-1)^{2m-1} = (\mu^2 - 1)^{2m-1} = \sum_{t=0}^{2m-1} \binom{2m-1}{t} (-1)^{2m-1-t} (\mu^2)^t = -1 + \mu^2 + \sum_{t=2}^{2m-1} \binom{2m-1}{t} (-1)^{2m-1-t} (\mu^2)^t.$$

then $f(k^*, \mu)$ can be rewritten as

$$f(k^*, \mu) = \frac{\left(1 - \frac{k^*}{2p} + \frac{k^*}{2p}\mu^2\right) \mu^{2(k^*-2p)}}{(k^*-2p)!p!(p-1)!2^{2p-1}} \left(-1 + \mu^2 \right)$$

$$+ \sum_{t=2}^{2p-1} \binom{2p-1}{t} (-1)^{2p-1-t} (\mu^2)^t + \sum_{m=1}^{p-1} \frac{\left(1 + \frac{k^*(r-1)}{2m}\right) \mu^{2(k^*-2m)} (r-1)^{2m-1}}{(k^*-2m)!m!(m-1)!2^{2m-1}}$$

$$f(k^*, \mu) = \begin{cases} \frac{\mu^2 \left(-1 + \mu^2 + \sum_{t=2}^{2p-1} \binom{2p-1}{t} (-1)^{2p-1-t} (\mu^2)^t \right)}{p!(p-1)!2^{2p-1}} + \tilde{f}(k^*, \mu) & \text{if } k^* = 2p, \\ \frac{\left(-\frac{1}{2p} + \left(\frac{1}{2p} + 1\right)\mu^2 \right) \left(-1 + \mu^2 + \sum_{t=2}^{2p-1} \binom{2p-1}{t} (-1)^{2p-1-t} (\mu^2)^t \right) \mu^2}{p!(p-1)!2^{2p-1}} + \tilde{f}(k^*, \mu) & \text{if } k^* = 2p+1, \end{cases}$$

with

$$\tilde{f}(k^*, \mu) = \sum_{m=1}^{p-1} \frac{\left(1 + \frac{k^*(r-1)}{2m}\right) \mu^{2(k^*-2m)} (r-1)^{2m-1}}{(k^*-2m)!m!(m-1)!2^{2m-1}}.$$

Let's call $f_0(k^*, \mu)$ the part of $f(k^*, \mu)$ that contains the lowest power of μ , $f_0(k^*, \mu)$ is given by

$$f_0(k^*, \mu) = \begin{cases} -\frac{\mu^2}{p!(p-1)!2^{2p-1}}, & \text{if } k^* = 2p, \\ \frac{\mu^2}{(2p)p!(p-1)!2^{2p-1}}, & \text{if } k^* = 2p+1. \end{cases} \quad (70)$$

Having assembled all the necessary ingredients, we are now ready to proceed with the proof.

Proof. Proof of Proposition 2.

Let's call $k^* = 2p + 1 \geq 3$, the Hermite degree. Using (69), let's consider μ such that

$$1 + \frac{k^*(\mu^2 - 1)}{2} > 0 \Leftrightarrow \mu^2 > 1 - \frac{2}{k^*} \Leftrightarrow \mu > \mu_0, \quad (71)$$

with $\mu_0 = \sqrt{1 - \frac{2}{k^*}} \in (0, 1)$. Now consider $\mu > \mu_0$ therefore $\forall m \in \{1, \dots, p\}$ the following hold

$$\begin{cases} 1 + \frac{k^*(\mu^2 - 1)}{2m} > 0 \\ (r-1)^{2m-1} < 0 \end{cases} \implies f(k^*, \mu) < 0. \quad (72)$$

Using (68) one can therefore concludes that $\forall \mu > \mu_0, A(\mu) > 0$.

Using (70) and (68), for $\mu = \varepsilon > 0$ with ε in the neighbourhood of zero, we have

$$\begin{aligned} \frac{k^*!}{k^*} \varepsilon^{-1} f(k^*, \varepsilon) &= \frac{(2p+1)!}{(2p+1)} \frac{\varepsilon}{(2p)p!(p-1)!2^{2p-1}} + O(\varepsilon^2) \\ &\implies A(\varepsilon) = -\frac{(2p+1)!}{(2p+1)} \frac{\varepsilon}{(2p)p!(p-1)!2^{2p-1}} + O(\varepsilon^2) < 0. \end{aligned} \quad (73)$$

Since A is continuous on $(0, 1)$ and changes sign on this interval, there exists $\tilde{\mu} \in (0, 1)$ such that $A(\tilde{\mu}) = 0$.

□

Proof. Proof of Proposition 3.

Using (69) and (70), one can show that when μ is in the neighborhood of zero, $f(k^*, \mu)$ becomes

$$\frac{k^*!}{k^*} \mu^{-1} f(k^*, \mu) = \begin{cases} -\frac{(2p)!}{2p} \frac{\mu}{p!(p-1)!2^{2p-1}} + O(\mu^2), & \text{if } k^* = 2p, \\ \frac{(2p+1)!}{2p+1} \frac{\mu}{(2p)p!(p-1)!2^{2p-1}} + O(\mu^2), & \text{if } k^* = 2p+1. \end{cases} \quad (74)$$

Now given that $k^* > 2$ one obtains the following

$$A = -\left(\mu^{k^*-1}(-1 + \mu^{k^*}) + \frac{k^*!}{k^*} \mu^{-1} f(k^*, \mu)\right) = \begin{cases} \frac{(2p)!}{2p} \frac{\mu}{p!(p-1)!2^{2p-1}} + O(\mu^2), & \text{if } k^* = 2p, \\ -\frac{(2p+1)!}{2p+1} \frac{\mu}{(2p)p!(p-1)!2^{2p-1}} + O(\mu^2), & \text{if } k^* = 2p+1, \end{cases} \quad (75)$$

$$B = -\left[\mu^{2k^*-2} + \frac{k^*!}{k^*} \mu^{-2} f(k^*, \mu)\right] = \begin{cases} \frac{(2p)!}{2p} \frac{1}{p!(p-1)!2^{2p-1}} + O(\mu^2), & \text{if } k^* = 2p, \\ -\frac{(2p+1)!}{2p+1} \frac{1}{p!(p-1)!(2p)2^{2p-1}} + O(\mu^2), & \text{if } k^* = 2p+1. \end{cases} \quad (76)$$

In the regime $\mu \rightarrow 0^+$, let's call A_0 and B_0 respectively the leading order of A and B . Using (60) we get

$$\sqrt{B_0^2 + 4A_0^2} = |B_0| \left(1 + \frac{4A_0^2}{B_0^2}\right)^{1/2} = |B_0| \left(1 + \frac{2A_0^2}{B_0^2}\right) = |B_0|(1 + \frac{2A_0^2}{B_0^2}),$$

which leads to

$$\frac{-B_0 + |B_0| \left(1 + \frac{2A_0^2}{B_0^2}\right)}{2A_0^2} = \frac{-B_0 + |B_0|}{2A_0^2} + \frac{|B_0|}{B_0^2} = \begin{cases} \frac{1}{B_0} & \text{if } B_0 > 0, \\ -\frac{B_0}{A_0^2} + \frac{1}{|B_0|} & \text{if } B_0 < 0. \end{cases}$$

One finally obtains

$$\tau(\mu) \sim \begin{cases} \frac{1}{B_0}, & \text{if } k^* = 2p \text{ with } p > 1, \\ -\frac{B_0 p! (p-1)! (2p) 2^{2p-1}}{(2p+1)!} \frac{1}{\mu^2}, & \text{if } k^* = 2p+1 \text{ with } p > 1. \end{cases} \quad (77)$$

From (69) we have that $f(k^*, \mu)$ is expressed as a positive powers of $\mu^2 - 1$ (we recall that $r = \mu^2$). In the regime $\mu^2 \rightarrow 1$, we have

$$f(k^*, \mu) = \sum_{m=1}^p \frac{\left(1 + \frac{k^*(r-1)}{2m}\right) \mu^{2(k^*-2m)} (r-1)^{2m-1}}{(k^*-2m)! m! (m-1)! 2^{2m-1}} = \frac{\mu^{2(k^*-2)} (\mu^2 - 1)}{(k^*-2)! 2} + O((\mu^2 - 1)^2), \quad (78)$$

$$-1 + \mu^{k^*} = \frac{k^*}{2} (\mu^2 - 1) + O((\mu^2 - 1)^2), \quad (79)$$

which leads to

$$\begin{aligned} A &= -\left(\frac{k^*}{2} (\mu^2 - 1) \mu^{k^*-1} + \frac{k^*-1}{2\mu} \mu^{2(k^*-2)} (\mu^2 - 1) + O((\mu^2 - 1)^2)\right) = a_1(\mu) \varepsilon + O(\varepsilon^2) \\ B &= -\left(\mu^{2k^*-2} + \frac{k^*-1}{2\mu^2} \mu^{2(k^*-2)} (\mu^2 - 1) + O((\mu^2 - 1)^2)\right) = b_0(\mu) + b_1(\mu) \varepsilon + O(\varepsilon^2), \end{aligned}$$

with $\varepsilon = \mu^2 - 1$, $a_1(\mu) = -\frac{k^*}{2} \mu^{k^*-1} - \frac{k^*-1}{2\mu} \mu^{2(k^*-2)}$, $b_0(\mu) = -\mu^{2k^*-2}$ and $b_1(\mu) = -\frac{k^*-1}{2\mu^2} \mu^{2(k^*-2)}$.

One then has

$$\begin{aligned} \tau(\mu) &= \frac{-(b_0(\mu) + b_1(\mu) \varepsilon) + \sqrt{(b_0(\mu) + b_1(\mu) \varepsilon)^2 + 4a_1^2(\mu) \varepsilon^2}}{2a_1^2(\mu) \varepsilon^2} = -\frac{b_0(\mu)}{a_1^2(\mu)} \frac{1}{\varepsilon^2} + O\left(\frac{1}{\varepsilon}\right) \\ &= \frac{\mu^{2k^*-2}}{\left(\frac{k^*}{2} \mu^{k^*-1} + \frac{k^*-1}{2\mu} \mu^{2(k^*-2)}\right)^2} \frac{1}{(\mu^2 - 1)^2} + O\left(\frac{1}{\mu^2 - 1}\right) \sim \frac{4}{(2k^*-1)^2} \frac{1}{(\mu^2 - 1)^2}. \end{aligned}$$

□

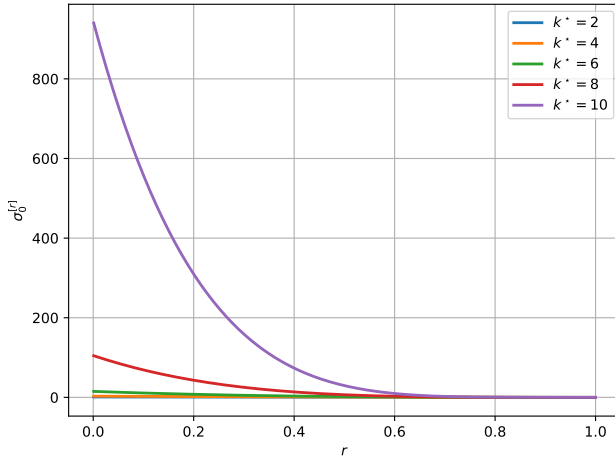


Figure 8. Mean student output (y-axis) for a pure Hermite activation of degree k^* as a function of the pre-activation variance (x-axis).

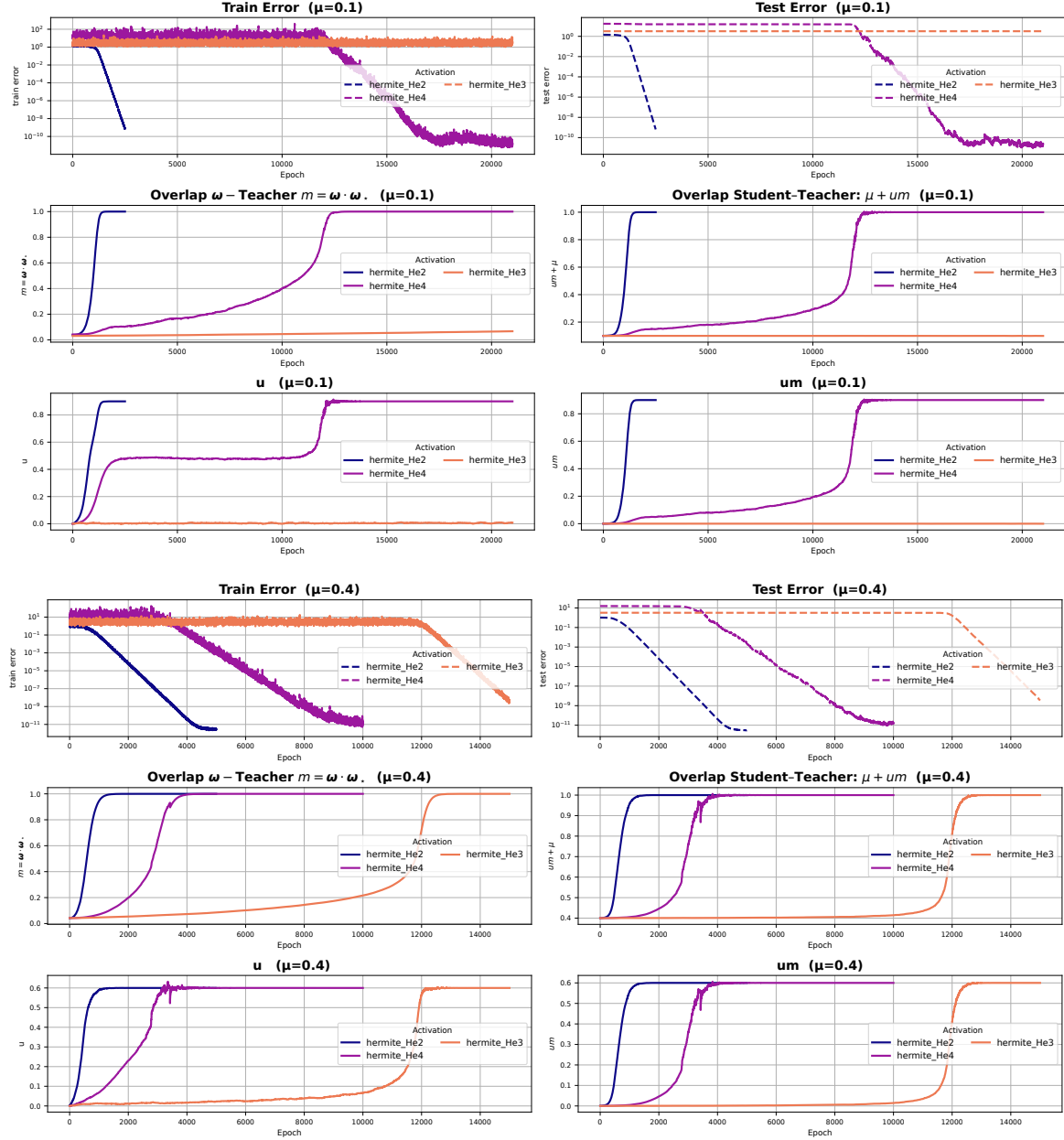


Figure 9. Learning dynamics of the student model (12) for different levels of pre-training alignment $\mu \in \{0.1, 0.4\}$, trained on data generated by the teacher model (11). We consider the matched teacher–student activation function to be Hermite polynomial with degree $k \in \{2, 3, 4\}$ as indicated in the legend. The student was trained using one-pass SGD with batch size $B = 1000$ and input dimension $d = 1000$. The panels report the dynamic of the test/train mean squared error (MSE), the alignment between the student and teacher directions $m = \omega_* \cdot \omega$, the effective teacher–student overlap $m_{\text{eff}} = \mu + um$, u and the product between overlap um . The results were average over three independent runs. The spherical constraint is enforced by normalizing ω after each gradient step and we used a learning rate $lr = 10^{-2} \times \delta_k$ with $\delta_k = 1/(k! \times k)$.

E.5. Effect of the mean for pure even Hermite activations

We consider the case in which the teacher activation function is a Hermite polynomial of degree k^* , and the student employs the same activation. As shown in (64), the Hermite coefficients of the student model depend on the parity of k^* . In particular, for odd degrees $k^* = 2p+1$, the first nonzero coefficient in the Hermite expansion is $\sigma_1^{[r]}$, whereas for even degrees $k^* = 2p$, it is $\sigma_0^{[r]}$. As a direct consequence, the mean of the activation satisfies $\mathbb{E}_{z \sim \mathcal{N}(0,r)}[\sigma(z)] = \begin{cases} 0, & \text{if } k^* = 2p+1, p \geq 1, \\ \sigma_0^{[r]}, & \text{if } k^* = 2p, p \geq 1, \end{cases}$ where we used the identity (30). For even-degree Hermite activations, the nonzero mean is $\sigma_0^{[r]} = k^*! \frac{(r-1)^{k^*/2}}{2^{k^*/2} (\frac{k^*}{2})!}$. This nonzero mean induces an additional contribution to the early-time dynamics of the order parameters u and m . Importantly, this effect vanishes continuously as $r \rightarrow 1$, as illustrated in Fig. 8.

In the regime considered in Appendix D.2, where $r \simeq \mu^2$, increasing the initial signal strength μ reduces the magnitude of the zeroth Hermite coefficient $\sigma_0^{[r]}$, and thus weakens the corresponding mean effect. Numerically, this manifests as the student dynamics after escaping the correlated search phase exhibiting an initial plateau for small μ , before escaping toward alignment, whereas this plateau progressively disappears as μ increases (see Fig. 9).

Numerical evidence of the effect of the presence of the mean on the dynamics of Hermite polynomials When considering Hermite activations, as predicted by our theory (cf. Figure 3), we observe that for odd degrees the escape time diverges as $\mu \rightarrow 0^+$, i.e., $\tau(\mu) \rightarrow +\infty$, whereas for even degrees the escape time τ remains finite. In the main text, we argued that this qualitative difference arises from the fact that students with even-degree Hermite activations exhibit a non-zero mean, while those with odd-degree activations do not. In Figure 9, we provide numerical evidence supporting this claim. Furthermore, Figure 8 illustrates how this mean depends on both μ and the Hermite degree. The key takeaway is that whenever the mean is non-vanishing, learning initially proceeds much faster; however, after this component is learned, the dynamics enter an extended plateau before higher-order features are eventually acquired.

F. A physical interpretation of LoRA dynamics

Using the linearized dynamics in the correlated search phase (8), which are fully characterized by the coefficients A and B , the evolution of the order parameters admits a useful interpretation in terms of an equivalent physical system near an unstable fixed point. In particular, we show that the effective dynamics in this regime are formally equivalent to those of a damped nonlinear oscillator. Such physics-inspired viewpoints have long been used in machine learning, both to motivate optimization algorithms and to provide theoretical insight into learning dynamics (Mézard et al., 1987; Choromanska et al., 2015; Mehta et al., 2019).

Concretely, the coupled first-order system in (8) can be rewritten as the second-order ordinary differential equation

$$\ddot{g}(t) - B \dot{g}(t) + \frac{\partial V}{\partial g} = 0, \quad (80)$$

which describes the motion of a particle in a one-dimensional nonlinear potential $V(g) = -A^2 \log(\cosh g)$. The relation $g(t) = \tanh^{-1} m(t)$ links the auxiliary variable g to the order parameter m , so that $g \rightarrow \pm\infty$ corresponds to $m \rightarrow \pm 1$. Within this mechanical analogy, the term proportional to \dot{g} acts as a linear velocity-dependent force: it is dissipative when $B < 0$, corresponding to effective damping, and amplifying when $B > 0$, corresponding to negative damping. Accordingly, B controls whether the dynamics locally dissipate or inject energy, while A sets the curvature of the potential and thus the strength of the signal-induced instability. Altogether, this suggests that the right part of the LoRA block primarily determines the effective directions and curvature that drive learning, while the left part mainly controls the time scale at which the dynamics progress along these directions. Detailed derivations are provided in Appendix F.1.

For linear activations, we have $A = (1 - \mu)$ and $B = -1$. In the physics interpretation, the dynamics are equivalent to a particle rolling down a cliff, initially placed at the top (cf. Fig. 10). Converging to the global minimizer corresponds to the particle moving away from the top of the cliff. The parameter A controls the slope of the cliff, implying that smaller values of μ correspond to steeper slopes and therefore faster escape from the top. The parameter B , on the other hand, acts as an additional force applied to the particle during its descent: a negative value of B corresponds to a dissipative (damping) force, whereas a positive value would correspond to an amplifying (impulsive) force. See Appendix F.1 for detailed derivations.

F.1. Proof of the physics interpretation of the linearized dynamics

Our analysis holds in the regime described in Appendix D.2, where higher-order powers of the order parameters can be neglected. In this regime, the learning dynamics are governed by the closed system of ordinary differential equations given in Eq. (57). Since these equations are linear in the order parameters, they define a system of first-order linear differential equations. In this appendix, we show that this system can be recast as a second-order differential equation, which admits a natural interpretation as a one-dimensional dissipative mechanical system.

Change of variables. We introduce the following change of variables:

$$m(t) = \tanh g(t), \quad (81)$$

where $g(t) \in \mathbb{R}$. Differentiating with respect to time yields

$$\dot{m}(t) = \dot{g}(t) \cosh^{-2} g(t) = \dot{g}(t)(1 - m(t)^2). \quad (82)$$

In the linearized regime considered in Appendix D.2, the overlap $m(t)$ remains small throughout the search phase, so that $m(t)^2 \ll 1$. As a consequence, we may approximate

$$\dot{m}(t) \simeq \dot{g}(t). \quad (83)$$

Derivation of the second-order equation. Using the second dynamical equation in (57), differentiating once more with respect to time gives

$$\ddot{g}(t) = A\dot{u}(t).$$

From Eq. (57), the evolution of $u(t)$ is

$$\dot{u}(t) = Bu(t) + Am(t).$$

Substituting this expression into the equation for $\ddot{g}(t)$ and using $u(t) \simeq \dot{g}(t)$, we obtain

$$\ddot{g}(t) = A(Bu(t) + Am(t)) = B\dot{g}(t) + A^2 \tanh g(t).$$

Rearranging terms, we arrive at the second-order differential equation

$$\ddot{g}(t) - B\dot{g}(t) - A^2 \tanh g(t) = 0. \quad (84)$$

Mechanical interpretation. Equation (84) can be written in Newtonian form with a velocity-dependent force:

$$\ddot{g}(t) - B\dot{g}(t) + \frac{\partial V(g)}{\partial g} = 0, \quad (85)$$

where the effective potential $V(g)$ is

$$V(g) = -A^2 \log(\cosh g). \quad (86)$$

This representation interprets the learning dynamics as the motion of a particle in a one-dimensional potential $V(g)$, subject to a linear force proportional to the velocity. Importantly, this term is *dissipative* only when $B < 0$ (effective friction), while it becomes *amplifying* when $B > 0$ (negative friction).

This distinction is made explicit by introducing the associated mechanical energy

$$E(t) := \frac{1}{2}\dot{g}(t)^2 + V(g(t)). \quad (87)$$

Differentiating and using the equation of motion yields

$$\frac{d}{dt}E(t) = \dot{g}(t)\ddot{g}(t) + V'(g(t))\dot{g}(t) = \dot{g}(t)(\ddot{g}(t) + V'(g(t))) = B\dot{g}(t)^2. \quad (88)$$

Therefore, if $B < 0$ then $\dot{E}(t) \leq 0$ and the dynamics monotonically dissipate energy, consistent with a frictional interpretation. Conversely, if $B > 0$ then $\dot{E}(t) \geq 0$ and the velocity-dependent term injects energy into the system, leading to effective self-amplification. Hence, the qualitative behavior (plateaus, instabilities, and escape times) is governed by the competition between the driving set by the potential shape (controlled by A) and the sign and magnitude of the velocity-dependent term controlled by B .

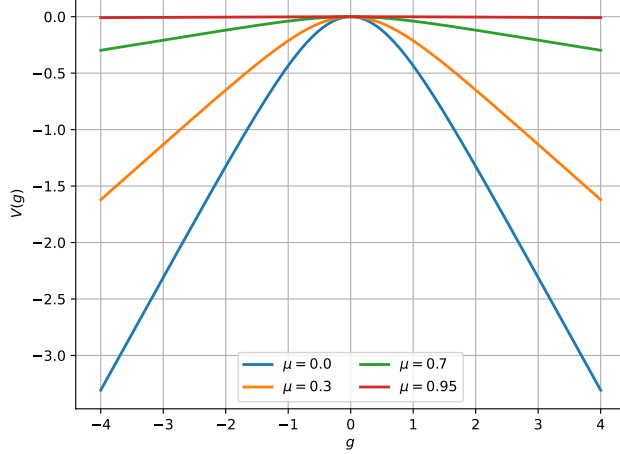


Figure 10. Effective potential for linear activation

Case of linear activation When both the teacher and the student use a linear activation function, the coefficients reduce to $B = -1$ and $A = 1 - \mu$, and Eq. (84) becomes

$$\ddot{g}(t) + \dot{g}(t) - (1 - \mu)^2 \tanh g(t) = 0. \quad (89)$$

This is a nonlinear second-order ordinary differential equation.

- **Case $\mu = 1$.** When $\mu = 1$, the nonlinear term vanishes and Eq. (89) reduces to a linear equation, which admits the explicit solution

$$g(t) = g_0 + \dot{g}_0(1 - e^{-t}).$$

In terms of the original order parameters, this corresponds to

$$u(t) = u_0 e^{-t}, \quad m(t) = m_0.$$

Hence, $u(t) \rightarrow 0$ as $t \rightarrow \infty$, while the overlap $m(t)$ remains frozen at its initial value. For a random initialization $\omega \sim \text{Unif}(\mathbb{S}^{d-1})$, we have $m_0 = O(d^{-1/2})$, so that the initial alignment vanishes in the large- d limit with high probability. In this regime, the associated population loss satisfies $\mathcal{L}(u_0, m_0) = o(1)$ as $d \rightarrow +\infty$, indicating that the system is initialized in the vicinity of the teacher solution.

- **Case $0 \leq \mu < 1$.** For $\mu < 1$, Eq. (89) does not admit a closed-form analytical solution. Nevertheless, it admits a clear mechanical interpretation as the damped motion of a particle in the effective potential

$$V(g) = -(1 - \mu)^2 \log(\cosh g). \quad (90)$$

For any $\mu < 1$, this potential is concave and symmetric around $g = 0$, with a curvature that vanishes as $\mu \rightarrow 1$. A random initialization corresponds to $m \simeq 0$, and hence $g \simeq 0$, placing the particle near the unstable maximum of the potential. Perfect alignment corresponds to $m(t) = \pm 1$, or equivalently $g(t) \rightarrow \pm\infty$, which can be interpreted as the particle escaping from the top of the potential. The convergence rate toward alignment is controlled by the competition between the potential-induced instability (cf. Fig. 10), parametrized by $(1 - \mu)^2$, and the effective damping coefficient, which in this case is equal to 1.

G. Descent phase

In this section, we aim to provide mathematical results showing that, once the dynamics enter the *descent phase*, they necessarily converge toward a global minimizer of the population loss. Our results are built on the following assumption on the population loss.

Assumption 2 (Population loss). There exist $\eta \in (0, 1)$ and $c > 0$ such that, for all $u, m \in \mathbb{R}$ with $|m| \in [\eta, 1]$, $\text{sign}(m) \partial_m \mathcal{L}(u, m) \leq -c$.

In this phase, at least one of the order parameters scales with μ , so that the linear approximation used in the correlated search phase is no longer valid and the full structure of the population loss must be taken into account. The dynamics of the order parameters in the descent phase are governed by

$$\dot{m} = -\phi_m(u, m)(1 - m^2), \quad \dot{u} = -\phi_u(u, m), \quad (91)$$

where $\phi_m := \partial_m \mathcal{L}(u, m)$ and $\phi_u := \partial_u \mathcal{L}(u, m)$.

The population loss $\mathcal{L}(u, m)$ acts as a Lyapunov function for the flow (91). Taking its time derivative along the trajectories yields

$$\frac{d\mathcal{L}(u, m)}{dt} = -\phi_u(u, m)^2 - \phi_m(u, m)^2(1 - m^2) \leq 0, \quad (92)$$

with equality if and only if $\phi_u(u, m) = 0$ or $|m| = 1$. Equation (92) shows that the dynamics monotonically decrease the population loss. Since both u and m are nontrivial along the trajectory, the dynamics converge to a minimizer of the population loss. The following result guarantees that, in the descent phase, the overlap satisfies $|m| \rightarrow 1$.

Proposition 4. *Assume that Assumption 2 holds, and let $(u(t), m(t))$ be a solution of (91) with $|m(t_0)| \in [\eta, 1)$ for some $t_0 \geq t_{\text{exit}}$. Then there exists a constant $c > 0$ (depending only on \mathcal{L}) such that, for all $t \geq t_0$,*

$$1 - |m(t)| \leq (1 - |m(t_0)|) e^{-2c(t-t_0)}. \quad (93)$$

In particular, $|m(t)| \rightarrow 1$ exponentially fast as $t \rightarrow \infty$, and the sign of $m(t)$ remains constant for all $t \geq t_0$.

We showed above that $|m(t)| \rightarrow 1$. It remains to characterize the asymptotic behavior of the scalar parameter u . It is important to keep in mind that, although $|m| = 1$, in the presence of teacher-student activation mismatch the global minimizer of the population loss does not necessarily correspond to recovery of the ground-truth direction, meaning that $m_{\text{eff}} = \mu + um \neq \pm 1$. Therefore, full recovery of the teacher direction is guaranteed only in the matching case $\phi(\cdot) = \sigma(\cdot)$. To prove this, we require the following assumption.

Assumption 3 (Slice well-posedness and sign-identifiability). Assume the matching setting $\sigma = \phi$. The activation $\sigma : \mathbb{R} \rightarrow \mathbb{R}$ is locally Lipschitz (hence differentiable a.e.) and of at most polynomial growth, so that the slice losses defined below are finite and C^1 in u .

Fix $s \in \{-1, +1\}$ and define the slice loss

$$\mathcal{L}(u, s) = \mathbb{E} \left[(\sigma(\lambda_{\star}) - \sigma((\mu + us)\lambda_{\star}))^2 \right], \quad \lambda_{\star} \sim \mathcal{N}(0, 1).$$

We assume:

- i) **Convex slice with bounded sublevel sets (no escape to infinity).** For each $s \in \{-1, +1\}$, the map $u \mapsto \mathcal{L}(u, s)$ is convex. Moreover, for the relevant loss level $\ell_0 := \mathcal{L}(u(t_0), s)$ (with t_0 as in Proposition 5), the sublevel set $\{u \in \mathbb{R} : \mathcal{L}(u, s) \leq \ell_0\}$ is bounded.
- ii) **No nontrivial scaling symmetries.** If there exists $a \neq 0$ such that $\sigma(az) = \sigma(z)$ for all $z \in \mathbb{R}$, then $a \in \{-1, +1\}$.
- iii) **Realizability on the slice.** For each $s \in \{-1, +1\}$, the minimum is attained at zero loss: $\min_u \mathcal{L}(u, s) = 0$.

Remark 4. Convexity in Assumption 3 is not assumed to be strict; in particular, when σ is even, the slice loss may admit two global minimizers.

Under this assumption, the following proposition holds.

Proposition 5. *Assume the matching teacher-student setting $\sigma = \phi$ and that Assumption 3 holds. Let $(u(t), m(t))$ be any solution of (91) such that $m(t) \rightarrow s \in \{-1, +1\}$ as $t \rightarrow \infty$.*

Then $u(t)$ converges to a global minimizer of the slice loss $\mathcal{L}(\cdot, s)$. Moreover,

$$u(t) \rightarrow \begin{cases} s(1 - \mu), & \text{if } \sigma \text{ is not even,} \\ s(1 - \mu) \text{ or } s(-1 - \mu), & \text{if } \sigma \text{ is even.} \end{cases}$$

Remark 5. In the matching activation setting, the above propositions guarantee that once the dynamics escape the correlated search phase, they converge so as to recover the teacher direction. No such guarantee can be made in the presence of activation mismatch between teacher and student. Proofs of Propositions 4 and 5 are provided in Appendix G.1.

G.1. Descent phase: proof of Proposition 4 and Proposition 5

Proof. Proof of Proposition 4. Write $\phi_m(u, m) = \partial_m \mathcal{L}(u, m)$ and define

$$h(u, m) := -\phi_m(u, m) = -\partial_m \mathcal{L}(u, m).$$

By Assumption 2, for all u and all m with $|m| \in [\eta, 1]$,

$$\text{sign}(m) \partial_m \mathcal{L}(u, m) \leq -c, \quad \text{so that} \quad -\text{sign}(m) \partial_m \mathcal{L}(u, m) \geq c.$$

The m -dynamics in (91) is

$$\dot{m} = -\phi_m(u, m) (1 - m^2) = -\partial_m \mathcal{L}(u, m) (1 - m^2).$$

For $t \geq t_0$, since $|m(t_0)| \in (\eta, 1)$ and the drift always pushes $|m|$ away from zero in the region $|m| \in [\eta, 1]$, we have $|m(t)| \in [\eta, 1]$ and $\text{sign}(m(t)) = \text{sign}(m(t_0))$ for all $t \geq t_0$.

Set $s(t) := |m(t)|$. Then

$$\dot{s}(t) = \frac{d}{dt} |m(t)| = \text{sign}(m(t)) \dot{m}(t) = -\text{sign}(m(t)) \partial_m \mathcal{L}(u(t), m(t)) (1 - m(t)^2).$$

Using the assumption $-\text{sign}(m) \partial_m \mathcal{L}(u, m) \geq c$ for $|m| \in [\eta, 1]$ and the identity $1 - m(t)^2 = 1 - s(t)^2$, we obtain

$$\dot{s}(t) \geq c(1 - s(t)^2).$$

Define $g(t) := 1 - s(t)$. Then

$$\begin{aligned} \dot{g}(t) &= -\dot{s}(t) \leq -c(1 - s(t)^2) \\ &= -c(1 - s(t))(1 + s(t)) \leq -c(1 + \eta)g(t), \end{aligned}$$

since $s(t) \geq \eta$ for all $t \geq t_0$. Renaming $2c := c(1 + \eta)$ (i.e., absorbing constants into c), we obtain

$$\dot{g}(t) \leq -2cg(t).$$

By Grönwall's inequality, for all $t \geq t_0$,

$$g(t) \leq g(t_0) e^{-2c(t-t_0)},$$

that is,

$$1 - |m(t)| \leq (1 - |m(t_0)|) e^{-2c(t-t_0)}.$$

Hence $|m(t)| \rightarrow 1$ exponentially fast as $t \rightarrow \infty$, and the sign of $m(t)$ cannot change after t_0 . \square

By Proposition 4, in the descent phase we have $|m(t)| \rightarrow 1$ and the sign of $m(t)$ is constant. We now show that, conditional on $m(t) \rightarrow s \in \{-1, 1\}$, the scalar parameter $u(t)$ converges to the corresponding optimal value $s(1 - \mu)$.

Proof. Proof of Proposition 5. Fix $s \in \{-1, 1\}$. In the matching-activation case $\sigma = \phi$, and for $m = s$, the population loss along the teacher direction can be written as

$$\mathcal{L}(u, s) = \mathbb{E}_{\lambda_*} \left[(\sigma(\lambda_*) - \sigma((\mu + us)\lambda_*))^2 \right], \quad \lambda_* \sim \mathcal{N}(0, 1),$$

which is nonnegative.

Moreover, by definition, $\mathcal{L}(s(1 - \mu), s) = 0$, and, if σ is even, also $\mathcal{L}(s(-1 - \mu), s) = 0$. Hence $\min_u \mathcal{L}(u, s) = 0$.

We first show convergence to the set of global minimizers. Along the dynamics (91), we have

$$\frac{d}{dt} \mathcal{L}(u(t), m(t)) = \phi_u(u, m) \dot{u} + \phi_m(u, m) \dot{m} = -\phi_u(u, m)^2 - (1 - m^2)\phi_m(u, m)^2 \leq 0.$$

Therefore, $\mathcal{L}(u(t), m(t))$ is nonincreasing and bounded from below, and thus converges as $t \rightarrow \infty$. By Assumption 3 (i), the slice loss $u \mapsto \mathcal{L}(u, s)$ is convex and has bounded sublevel sets. Since $\mathcal{L}(u(t), s)$ is nonincreasing along the trajectory, it follows that $u(t)$ remains in a bounded sublevel set and therefore remains bounded for all $t \geq t_0$. Consequently, the trajectory admits limit points.

Let (u_∞, m_∞) be any limit point. Since $m(t) \rightarrow s$ by hypothesis, we have $m_\infty = s$. Moreover, since $\mathcal{L}(u(t), m(t))$ converges and its derivative is a sum of negative squares, it follows that

$$\phi_u(u(t), m(t)) \rightarrow 0 \quad \text{as } t \rightarrow \infty.$$

By continuity of ϕ_u and the fact that $m(t) \rightarrow s$, any limit point u_∞ of $u(t)$ satisfies $\phi_u(u_\infty, s) = 0$. Since $u \mapsto \mathcal{L}(u, s)$ is convex, every critical point is a global minimizer, hence $u_\infty \in \arg \min_u \mathcal{L}(u, s)$. Because the trajectory $u(t)$ is bounded and all its limit points belong to the set of minimizers, we conclude that $u(t)$ converges to a global minimizer of $\mathcal{L}(\cdot, s)$.

It remains to identify the minimizers. Let u be such that $\mathcal{L}(u, s) = 0$. Then

$$\sigma((\mu + us)z) = \sigma(z) \quad \text{for a.e. } z \in \mathbb{R}.$$

By Assumption 3 (ii), this implies $\mu + us \in \{-1, +1\}$. If σ is not even, the identity $\sigma(-z) = \sigma(z)$ fails, so the case $\mu + us = -1$ is impossible, and the only minimizer is $u = s(1 - \mu)$. If σ is even, both $\mu + us = \pm 1$ are admissible, yielding the two minimizers $u = s(1 - \mu)$ and $u = s(-1 - \mu)$.

Therefore,

$$u(t) \rightarrow \begin{cases} s(1 - \mu), & \text{if } \sigma \text{ is not even,} \\ s(1 - \mu) \text{ or } s(-1 - \mu), & \text{if } \sigma \text{ is even.} \end{cases}$$

□

H. The role of the loss function

So far, our analysis has focused on the mean squared loss. In this appendix, we investigate how the choice of a different loss function affects the role played by the signal strength μ . More precisely, we consider the correlation loss

$$\ell(\hat{y}, y) = 1 - \hat{y}y, \tag{94}$$

which belongs to the correlated statistical query (CSQ) family and was also employed in recent work such as [Damian et al. \(2023\)](#); [Gerace et al. \(2024\)](#); [Arnaboldi et al. \(2024\)](#).

We consider the teacher–student setting with linear activation functions for both the teacher and the student. In this case, the population loss takes the form

$$\mathcal{L}(u, m) := \mathbb{E}_x \left[1 - (\omega_* \cdot x) ((\mu \omega_* + u \omega) \cdot x) \right] = 1 - \mu - um, \tag{95}$$

where $m := \omega \cdot \omega_*$ denotes the overlap between the student direction ω and the teacher direction ω_* .

The gradients of the population loss with respect to the order parameters u and m are given by

$$\frac{\partial \mathcal{L}}{\partial u} = -m, \quad \frac{\partial \mathcal{L}}{\partial m} = -u. \tag{96}$$

Notably, the gradient of the population loss is completely independent of the signal strength μ .

Interpretation. In the setting considered here, the fact that the population gradient does not depend on μ has a direct and striking consequence: an arbitrarily strong planted component of the teacher direction ω_* in the student model does not influence the learning dynamics. In other words, the optimization problem behaves as if it were effectively blind to the initial signal encoded by μ . This behavior is in sharp contrast with what is observed when using the quadratic loss, where the signal strength μ plays a crucial role in shaping the learning dynamics and the escape from the search phase. The key observation here concerns the structure of the population gradient field, which remains entirely independent of the signal strength μ . The present observation suggests that, in practical scenarios such as LoRA fine-tuning, the choice of the loss function can play a non-trivial and sometimes dominant role in determining whether and how the pre-trained weight is exploited during learning.

I. The role of the rank

We now move beyond the single-index setting and consider a more realistic LoRA scenario, in which the goal is to reconstruct a *matrix* of teacher directions $\omega^* \in \mathbb{R}^{K \times d}$ in a committee-machine-like model recently studied in (Barbier et al., 2025). Our aim is to show that the LoRA rank primarily shapes the descent phase of the dynamics, whereas the pre-trained weights control the rate at which the search phase is escaped. Although our theoretical analysis focuses on linear activations, we observe experimentally in Figure 11 that this qualitative picture persists for nonlinear activations.

Data generation. The data are generated according to a noiseless teacher model

$$y(\mathbf{x}) = \frac{1}{\sqrt{K}} \sum_{k=1}^K \omega_k^* \cdot \mathbf{x}, \quad (97)$$

where $\mathbf{x}_i \sim \mathcal{N}(0, I_d)$, the teacher weights satisfy $\omega_k^* \in \mathbb{S}^{d-1}$ and $\omega_k^* \cdot \omega_{k'}^* = \delta_{kk'}$, and $\sigma : \mathbb{R} \rightarrow \mathbb{R}$ is a generic activation function.

LoRA student model. We consider a simplified LoRA-style parameterization of the student in which each teacher direction is initialized with a correlated component and adapted through a shared low-rank update. Specifically, for rank R , let $\mathbf{U} \in \mathbb{R}^{K \times R}$ and $\omega \in \mathbb{R}^{d \times R}$, with columns

$$\omega = [\omega^{(1)}, \dots, \omega^{(R)}], \quad \mathbf{U} = [u^{(1)}, \dots, u^{(R)}].$$

The effective weight vector associated with neuron k is

$$\tilde{\omega}_k = \mu_k \omega_k^* + \sum_{r=1}^R u_{k,r} \omega^{(r)}, \quad \mu_k \in (0, 1), \quad (98)$$

where μ_k controls the strength of the pre-trained alignment with the k -th teacher direction. The corresponding student output is

$$\hat{y}(\mathbf{x}) = \frac{1}{\sqrt{K}} \sum_{k=1}^K \tilde{\omega}_k \cdot \mathbf{x}. \quad (99)$$

Order parameters. As usual, define the overlaps (for $r, s \in \{1, \dots, R\}$)

$$m_{k,r} := \omega_k^* \cdot \omega^{(r)}, \quad q_{rs} := \omega^{(r)} \cdot \omega^{(s)}, \quad \Delta_k := 1 - \mu_k.$$

We also introduce the rank- r ‘‘Gram’’ of the u ’s:

$$C_{rs} := \sum_{k=1}^K u_{k,r} u_{k,s} \quad (r, s \in \{1, \dots, R\}).$$

Population loss. The population loss is

$$\mathcal{L}(\omega, \mathbf{U}) = \frac{1}{2K} \mathbb{E}_x \left[(y(\mathbf{x}) - \hat{y}(\mathbf{x}))^2 \right] = \frac{1}{2K} \left\| \sum_{k=1}^K (\omega_k^* - \tilde{\omega}_k) \right\|^2 = \frac{1}{2K} \sum_{k=1}^K \left\| \Delta_k \omega_k^* - \sum_{r=1}^R u_{k,r} \omega^{(r)} \right\|^2.$$

Expanding and using $\omega_k^* \cdot \omega_{k'}^* = \delta_{kk'}$,

$$\mathcal{L}(\omega, \mathbf{U}) = \frac{1}{2K} \left[\sum_{k=1}^K \Delta_k^2 + \sum_{k=1}^K \sum_{r,s=1}^R u_{k,r} u_{k,s} q_{rs} - 2 \sum_{k=1}^K \sum_{r=1}^R \Delta_k u_{k,r} m_{k,r} \right]. \quad (100)$$

Gradient w.r.t. $u_{k,r}$. For each k and $r \in \{1, \dots, R\}$,

$$\frac{\partial \mathcal{L}}{\partial u_{k,r}} = \frac{1}{K} \left[\sum_{s=1}^R q_{rs} u_{k,s} - \Delta_k m_{k,r} \right]. \quad (101)$$

Gradient w.r.t. $\omega^{(r)}$. Working in \mathbb{R}^d ,

$$\nabla_{\omega^{(r)}} \mathcal{L} = \frac{1}{K} \left[\sum_{k=1}^K u_{k,r}^2 \omega^{(r)} + \sum_{k=1}^K u_{k,r} \sum_{s \neq r} u_{k,s} \omega^{(s)} - \sum_{k=1}^K \Delta_k u_{k,r} \omega_k^* \right] = \frac{1}{K} \left[\sum_{s=1}^R C_{rs} \omega^{(s)} - \sum_{k=1}^K \Delta_k u_{k,r} \omega_k^* \right], \quad (102)$$

where we used the definition of C_{rs} .

Spherical gradient flow (columns constrained on the sphere). Assume each column is constrained to the sphere $\|\omega^{(r)}\|^2 = 1$ (equivalently $q_{rr} = 1$). Then the spherical (Riemannian) gradient is

$$\nabla_{\omega^{(r)}}^S \mathcal{L} = \left(I - \omega^{(r)} \omega^{(r)\top} \right) \nabla_{\omega^{(r)}} \mathcal{L} = \left(I - \omega^{(r)} \omega^{(r)\top} \right) \nabla_{\omega^{(r)}} \mathcal{L},$$

and the continuous-time gradient flow is

$$\frac{du_{k,r}}{dt} = -\frac{\partial \mathcal{L}}{\partial u_{k,r}}, \quad \frac{d\omega^{(r)}}{dt} = -\nabla_{\omega^{(r)}}^S \mathcal{L}.$$

Induced dynamics for the overlaps. Differentiate $m_{k,r} = \omega_k^* \cdot \omega^{(r)}$:

$$\frac{dm_{k,r}}{dt} = -\omega_k^* \cdot \nabla_{\omega^{(r)}}^S \mathcal{L} = -\left(\omega_k^* - m_{k,r} \omega^{(r)} \right) \nabla_{\omega^{(r)}} \mathcal{L}.$$

Effective alignment and sufficient statistics. For teacher direction k , the component of the student along ω_k^* is

$$m_{k,\text{eff}} := \omega_k^* \cdot \tilde{\omega}_k = \mu_k + \sum_{r=1}^R u_{k,r} m_{k,r}, \quad (103)$$

so tracking the pairs $(u_{k,r}, m_{k,r})_{r=1}^R$ is sufficient to describe how much the k -th teacher direction is represented in the current model.

One summarizes the dynamics of the order parameters as follow

$$\begin{aligned} \frac{du_{k,r}}{dt} &= \frac{1}{K} \left[\Delta_k m_{k,r} - \sum_{s=1}^R q_{rs} u_{k,s} \right], \\ \frac{dm_{k,r}}{dt} &= \frac{1}{K} \left[\Delta_k u_{k,r} (1 - m_{k,r}^2) - \sum_{s \neq r}^R C_{rs} (m_{k,s} - m_{k,r} q_{rs}) \right]. \end{aligned} \quad (104)$$

When the cross-rank interaction terms $\sum_{s=1}^R q_{rs} u_{k,s}$ and $\sum_{s \neq r}^R C_{rs} (m_{k,s} - m_{k,r} q_{rs})$ are absent, the dynamics decouple across the rank index r : each pair $(m_{k,r}, u_{k,r})$ evolves independently according to the same two-dimensional system, and increasing the rank merely replicates identical learning channels without affecting the convergence rate. Once these terms

are present, however, increasing the rank R directly increases the number of contributions in the sums, thereby strengthening cross-rank interactions. As a consequence, the evolution of a given component $(m_{k,r}, u_{k,r})$ is no longer driven solely by its own alignment with the target, but is increasingly influenced by the state of the other LoRA components through the geometric couplings encoded in Q and the coefficient correlations encoded in C . This induces a qualitative change in the dynamics: while a larger rank provides more directions along which alignment can in principle build, it also promotes mixing and redistribution of the learning signal across ranks. As a result, the growth of individual overlaps can become less coherent, and the effective driving force acting on each component may be diluted. Consequently, increasing the LoRA rank does not necessarily accelerate convergence, since the benefit of additional adaptation directions can be offset by stronger cross-rank coupling that reshapes—and potentially slows—the collective dynamics.

Linearization around the correlated-search origin. We consider the early-time regime in which the LoRA coefficients and overlaps are small,

$$u_{k,r} \approx 0, \quad m_{k,r} \approx 0, \quad \text{and} \quad q_{rr} = 1, \quad q_{rs} \approx 0 \quad (r \neq s),$$

corresponding to LoRA directions that are (approximately) orthonormal and only weakly correlated with the teacher directions. In this regime, the coupling matrix $C_{rs} = \sum_{k=1}^K u_{k,r} u_{k,s}$ is quadratic in u (i.e. $C_{rs} = O(\|u\|^2)$), so the inter-rank coupling term in the exact overlap dynamics (104) disappears at linear order. Consequently, for each fixed pair (k, r) , the dynamics reduces to an independent 2×2 linear system,

$$\begin{cases} \frac{du_{k,r}}{dt} = \frac{1}{K} \left(-u_{k,r} + \Delta_k m_{k,r} \right), \\ \frac{dm_{k,r}}{dt} = \frac{1}{K} \Delta_k u_{k,r}, \end{cases} \quad (105)$$

which is the same linear block as in the rank-one case. Equivalently,

$$\frac{d}{dt} \begin{pmatrix} u_{k,r} \\ m_{k,r} \end{pmatrix} = \frac{1}{K} \underbrace{\begin{pmatrix} -1 & \Delta_k \\ \Delta_k & 0 \end{pmatrix}}_{=:A_k} \begin{pmatrix} u_{k,r} \\ m_{k,r} \end{pmatrix}.$$

The eigenvalues of the dynamics matrix $\frac{1}{K} A_k$ are therefore

$$\lambda_{k,\pm} = \frac{1}{2K} \left(-1 \pm \sqrt{1 + 4\Delta_k^2} \right) = \frac{1}{2K} \left(-1 \pm \sqrt{1 + 4(1 - \mu_k)^2} \right),$$

so the early growth/decay rates are identical to rank one, replicated across $r = 1, \dots, R$.

Interpretation: role of the rank and of the signal. Equation (105) shows that, at *linear order*, increasing the LoRA rank does not change the *per-mode* escape rate: the unstable eigenvalue $\lambda_{k,+}$ depends only on $\Delta_k = 1 - \mu_k$ (and on the width factor K), not on R (numerical evidence for linear and nonlinear activation in Figure 11). In other words, rank R provides R *independent channels* $(u_{k,r}, m_{k,r})$ through which alignment with direction k can start to grow, but each channel grows with the same intrinsic rate $\lambda_{k,+}$ near the origin. Rank becomes relevant beyond the linear regime, when the quadratic couplings (through C_{rs} and q_{rs}) turn on: then different LoRA directions compete/cooperate, potentially redistributing energy across ranks and changing the *nonlinear* transient, but not the linearized exponent.

The signal strength μ_k (equivalently $\Delta_k = 1 - \mu_k$) directly controls the *time scale* at which the dynamics escape the correlated search regime along direction k . Indeed, the unstable eigenvalue

$$\lambda_{k,+} = \frac{1}{2K} \left(-1 + \sqrt{1 + 4(1 - \mu_k)^2} \right)$$

induces a characteristic escape time

$$\tau_k(\mu_k) := \frac{1}{\lambda_{k,+}} = \frac{K(1 + \sqrt{1 + 4(1 - \mu_k)^2})}{2(1 - \mu_k)^2}. \quad (106)$$

This expression makes explicit that $\tau_k(\mu_k)$ diverges as $\mu_k \rightarrow 1$. When the pre-trained component is already strongly aligned with the teacher direction, the effective gradient signal driving further correction becomes vanishingly small, resulting in a slow drift and a prolonged correlated-search phase. Conversely, for weaker pre-training (smaller μ_k , hence larger $|1 - \mu_k|$), the escape time is shorter, allowing the dynamics to exit the search regime more rapidly and enter the descent phase.

Numerical evidence of the role of the rank In Figure 11, we provide evidence that the phenomenon of catastrophic overtraining persists in more complex settings, such as two-layer neural networks, and we further illustrate the effect of the LoRA rank. Details of the experimental setup are provided in the caption. As shown in Appendix I, for linear activations the rank plays no role during the search phase; consistently, in our numerical experiments increasing the rank does not fundamentally alter the observed dynamics. For nonlinear activations such as ReLU, the picture is more nuanced: while the escape from the search phase (i.e., departure from the initial plateau) occurs at approximately the same point across different ranks, the final performance achieved is rank-dependent. Moreover, in the ReLU setting, smaller values of μ (corresponding to weaker pre-training alignment) lead to an earlier escape from the search phase, although the asymptotic performance remains governed by the rank.

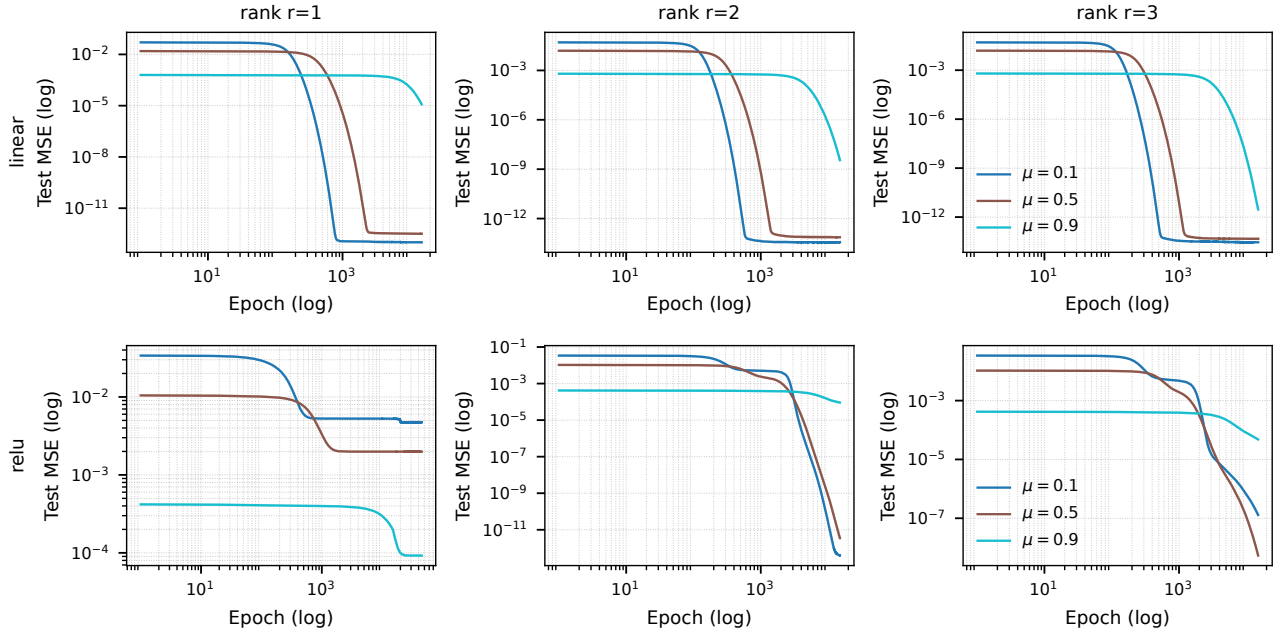


Figure 11. Learning dynamics of the student model (99). For the ReLU activation, we use a $1/K$ scaling for the output. The width of the hidden layer is set to $K = 4$. For the pre-trained weights, we consider $\tilde{\omega}_k = \mu \omega_k^* + \sum_{r=1}^R u_{k,r} \omega^{(r)}$, $k \in \{1, 2\}$, while for $k \geq 3$ we set $\tilde{\omega}_k = \omega_k^*$. We consider different levels of pre-training alignment $\mu \in \{0.1, 0.5, 0.9\}$ and train on data generated by the teacher model (97). We study matched teacher–student settings with linear and ReLU activations (from top to bottom), and train the student using one-pass SGD with batch size $B = 500$ and input dimension $d = 1000$. The panels report the test mean squared error (MSE), and, from left to right, the results for LoRA block ranks $r \in \{1, 2, 3\}$.

J. Numerical evidence of delayed learning near the singularity

Focusing on the Hermite-3 activation He_3 , we provide in Figure 12 numerical evidence of the effect of the pre-training alignment μ for a student model trained using one-pass SGD (further details of the numerical setup are given in the caption). As predicted by the theory and illustrated in Figure 3, the parameter μ has a non-trivial impact on the dynamics governing the escape from the correlated search phase. The observations reported here are fully consistent with the theoretical predictions. Crucially, near the singular regime at $\mu = 0.325$, a significant delay in escaping the search phase is observed numerically, in agreement with the theory. Across the different observables, we find that the quantity that exhibits a mild increase is the overlap m , while the LoRA coefficient u remains noisy during this stage.

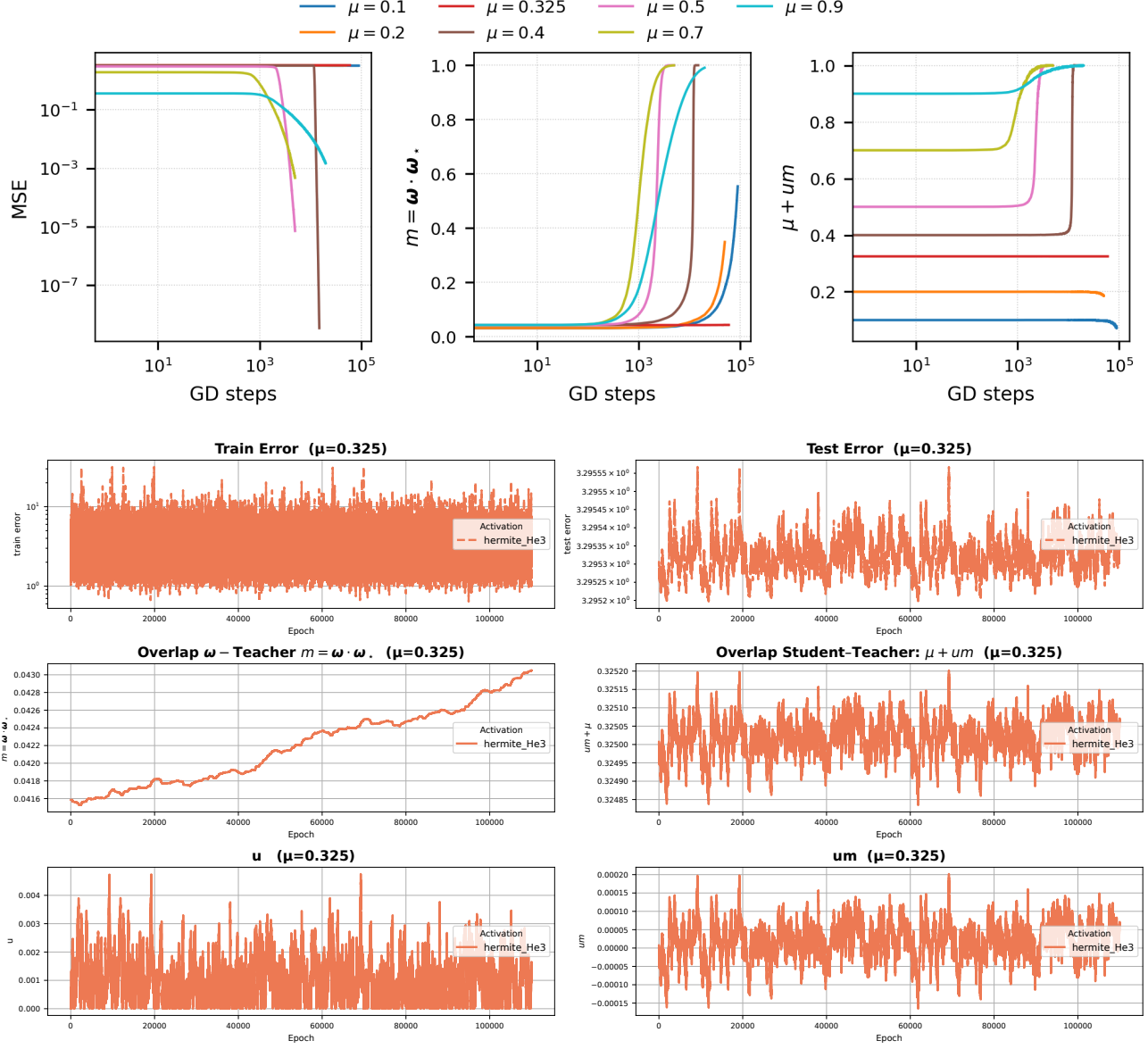


Figure 12. Learning dynamics of the student model (12) for different levels of pre-training alignment $\mu \in \{0.1, 0.2, 0.325, 0.4, 0.5, 0.7, 0.9\}$, trained on data generated by the teacher model (11). We consider the matched teacher-student activation function to be a Hermite polynomial of degree $k = 3$, as indicated in the legend. The student is trained using one-pass SGD with batch size $B = 1000$ and input dimension $d = 1000$. **Top:** the panels report the test mean squared error (MSE) (left), the alignment between the student and teacher directions $m = \omega_* \cdot \omega$ (middle), and the effective teacher-student overlap $m_{\text{eff}} = \mu + um$ (right). Results are averaged over three independent runs. A spherical constraint is enforced by normalizing ω after each gradient step, and the learning rate is set to $lr = 10^{-2} \delta_k$, with $\delta_k = 1/(k! k)$. As shown in the middle panel, the case $\mu = 0.325$, which lies close to the singular region (cf. the bottom panel of Fig. 3), exhibits a significantly longer escape time compared to the other values of μ . **Bottom:** from the second to the last row, the panels display a more detailed evolution of the observables: train/test error, the scalar parameter u , and the product um for the case $\mu = 0.325$.